Available online at www.sciencedirect.com

SciVerse ScienceDirect

Nuclear Physics B 866 (2013) 1–25

NUCLEAR PHYSICS B

www.elsevier.com/locate/nuclphysb

Nucleon mass and sigma term from lattice QCD with two light fermion flavors

QCDSF Collaboration

G.S. Bali [a], P.C. Bruns [a], S. Collins [a], M. Deka [a], B. Gläßle [a], M. Göckeler [a], L. Greil [a], T.R. Hemmert [a], R. Horsley [b], J. Najjar [a], Y. Nakamura [c], A. Nobile [d], D. Pleiter [a,d], P.E.L. Rakow [e], A. Schäfer [a], R. Schiel [a], G. Schierholz [f], A. Sternbeck [a,*], J. Zanotti [g]

[a] *Institut für Theoretische Physik, Universität Regensburg, 93040 Regensburg, Germany*
[b] *School of Physics, University of Edinburgh, Edinburgh EH9 3JZ, UK*
[c] *RIKEN Advanced Institute for Computational Science, Kobe, Hyogo 650-0047, Japan*
[d] *JSC, Research Center Jülich, 52425 Jülich, Germany*
[e] *Theoretical Physics Division, Department of Mathematical Sciences, University of Liverpool, Liverpool L69 3BX, UK*
[f] *Deutsches Elektronen-Synchrotron (DESY), 22603 Hamburg, Germany*
[g] *School of Chemistry and Physics, University of Adelaide, SA 5005, Australia*

Received 9 July 2012; accepted 8 August 2012

Available online 14 August 2012

Abstract

We analyze $N_f = 2$ nucleon mass data with respect to their dependence on the pion mass down to $m_\pi = 157$ MeV and compare it with predictions from covariant baryon chiral perturbation theory (BChPT). A novel feature of our approach is that we fit the nucleon mass data simultaneously with the directly obtained pion–nucleon σ-term. Our lattice data below $m_\pi = 435$ MeV is well described by $O(p^4)$ BChPT and we find $\sigma = 37(8)(6)$ MeV for the σ-term at the physical point. Using the nucleon mass to set the scale we obtain a Sommer parameter of $r_0 = 0.501(10)(11)$ fm.
© 2012 Elsevier B.V. All rights reserved.

Keywords: Nucleon mass; Pion–nucleon sigma term; Sommer scale; Covariant baryon chiral perturbation theory; Finite size corrections

* Corresponding author.
E-mail address: andre.sternbeck@ur.de (A. Sternbeck).

0550-3213/$ – see front matter © 2012 Elsevier B.V. All rights reserved.
http://dx.doi.org/10.1016/j.nuclphysb.2012.08.009

1. Introduction

Predicting low-energy hadronic properties is one basic goal of lattice QCD. A particular challenge to experiment as well as to theory is posed by the so-called pion–nucleon σ-term

$$\sigma = m_\ell \langle N|(\bar{u}u + \bar{d}d)|N\rangle \tag{1}$$

which parametrizes the light quark contribution to the nucleon mass. Here $m_\ell = m_u = m_d$ denotes the light quark mass.

At present, phenomenology does not give a clear picture of the magnitude of σ. A dispersion theoretical analysis led to $\sigma = 64(8)$ MeV [1], similar to the value $\sigma = 64(7)$ MeV obtained later in Ref. [2]. However the analysis of Ref. [3] suggested a much lower value, $\sigma = 45(8)$ MeV, which was also found in [4]. Recently, a new evaluation resulted in $\sigma = 59(7)$ MeV [5].

Calculating the pion–nucleon σ-term directly on the lattice is a computationally intensive task as it involves the computation of quark-line disconnected correlation functions. This has become feasible recently and was performed by us and others [6–8], though only at a single value of m_ℓ and of the lattice spacing a. An alternative, which has often been used in the past (see, e.g., the recent studies [8–11]), is given by the Feynman–Hellmann theorem. It allows us to express σ in terms of the derivative of the nucleon mass M_N with respect to m_ℓ:

$$\sigma = m_\ell \frac{\partial M_N}{\partial m_\ell}. \tag{2}$$

Calculating the nucleon mass on the lattice as a function of m_ℓ is relatively straightforward, but becomes expensive close to the physical point.

Until very recently, lattice QCD calculations have therefore been performed at rather large quark masses, such that results had to be extrapolated to the physical point over a wide range. Thanks to the efforts of different lattice QCD collaborations during the last years this situation has much improved. The QCDSF Collaboration, for example, has generated a large set of $N_f = 2$ gauge field configurations for a variety of quark masses, lattice spacings and volumes, reaching down to pion masses of about 157 MeV. These simulations employ the standard Wilson gauge action and the non-perturbatively $O(a)$ improved clover action for two flavors of mass-degenerate quarks.

In this paper we analyze nucleon mass data obtained from these simulations with respect to their quark-mass and volume dependence, compare this to $SU(2)$ covariant baryon chiral perturbation theory (BChPT), and extract a value for the pion–nucleon σ-term utilizing the Feynman–Hellmann theorem. A novel feature of our analysis is that we combine the nucleon mass data with a direct determination of the pion–nucleon σ-term [7], fitting both *simultaneously* to the corresponding $O(p^4)$ BChPT expressions. It turns out that this gives much more reliable and precise results compared to fits to the nucleon mass data only.

The outline of this article is as follows: In the next section we summarize and describe our lattice data. Our fitting procedure is described in Section 3. The results of the fits are then discussed in Section 4. In Section 5 we summarize the outcome of our analysis. In Appendix A we review the results from BChPT which underlie our analysis. Some more details on the fits can be found in Appendix B.

2. Lattice data

Our lattice data for the pseudoscalar (am_π) and nucleon mass (aM_N) were extracted from one-exponential fits to smeared–smeared correlators. For the smearing we used Jacobi smearing

Table 1
Lattice data for the pseudoscalar (am_π) and the nucleon mass (aM_N) in lattice units. In columns 6 and 7 we list the corresponding values in units of r_0. For am_π and aM_N we give the statistical errors, for $r_0 m_\pi$ ($r_0 M_N$) the errors are the combined statistical errors of r_0/a and am_π (aM_N). Stars in the first column mark all those entries which enter our fits [depending on the upper limit set for $(r_0 m_\pi)^2$].

β	κ	Lattice	am_π	aM_N	$r_0 m_\pi$	$r_0 M_N$	L/r_0
5.25	0.13460	$16^3 \times 32$	0.4932(10)	0.9436(49)	3.256(27)	6.230(59)	2.42
5.25	0.13520	$16^3 \times 32$	0.3821(13)	0.7915(55)	2.523(22)	5.226(56)	2.42
⋆ 5.25	0.13575	$24^3 \times 48$	0.2556(5)	0.6061(38)	1.687(14)	4.002(41)	3.63
⋆ 5.25	0.13600	$24^3 \times 48$	0.1840(7)	0.5088(72)	1.215(11)	3.359(55)	3.63
5.25	0.13620	$32^3 \times 64$	0.0997(11)	0.4012(87)	0.658(9)	2.649(61)	4.85
5.29	0.13400	$16^3 \times 32$	0.5767(11)	1.0546(51)	4.039(32)	7.386(67)	2.28
5.29	0.13500	$16^3 \times 32$	0.4206(9)	0.8333(32)	2.946(24)	5.836(50)	2.28
5.29	0.13550	$12^3 \times 32$	0.3605(32)	0.8325(96)	2.525(30)	5.831(81)	1.71
5.29	0.13550	$16^3 \times 32$	0.3325(14)	0.7020(72)	2.329(20)	4.916(63)	2.28
⋆ 5.29	0.13550	$24^3 \times 48$	0.3270(6)	0.6858(33)	2.290(18)	4.804(44)	3.43
5.29	0.13590	$12^3 \times 32$	0.3369(62)	0.8071(208)	2.360(47)	5.653(152)	1.71
5.29	0.13590	$16^3 \times 32$	0.2518(15)	0.6306(53)	1.763(17)	4.417(50)	2.28
⋆ 5.29	0.13590	$24^3 \times 48$	0.2395(5)	0.5554(46)	1.677(13)	3.890(44)	3.43
⋆ 5.29	0.13620	$24^3 \times 48$	0.1552(6)	0.4670(49)	1.087(10)	3.271(42)	3.43
5.29	0.13632	$24^3 \times 48$	0.1112(9)	0.4250(60)	0.779(9)	2.977(48)	3.43
5.29	0.13632	$32^3 \times 64$	0.1070(5)	0.3900(50)	0.750(7)	2.732(41)	4.57
⋆ 5.29	0.13632	$40^3 \times 64$	0.1050(3)	0.3810(30)	0.735(6)	2.669(29)	5.71
5.29	0.13640	$40^3 \times 64$	0.0660(8)	0.3708(196)	0.463(7)	2.597(139)	5.71
⋆ 5.29	0.13640	$48^3 \times 64$	0.0570(7)	0.3420(80)	0.399(6)	2.395(59)	6.85
5.40	0.13500	$24^3 \times 48$	0.4030(4)	0.7556(17)	3.339(30)	6.260(58)	2.90
5.40	0.13560	$24^3 \times 48$	0.3123(7)	0.6260(26)	2.588(24)	5.186(51)	2.90
5.40	0.13610	$24^3 \times 48$	0.2208(7)	0.5085(45)	1.829(17)	4.213(53)	2.90
5.40	0.13625	$24^3 \times 48$	0.1902(6)	0.4655(35)	1.576(15)	3.857(45)	2.90
5.40	0.13640	$24^3 \times 48$	0.1538(10)	0.4265(67)	1.274(14)	3.533(64)	2.90
⋆ 5.40	0.13640	$32^3 \times 64$	0.1505(5)	0.4163(44)	1.246(12)	3.449(48)	3.86
5.40	0.13660	$32^3 \times 64$	0.0845(6)	0.3530(71)	0.700(8)	2.924(64)	3.86
⋆ 5.40	0.13660	$48^3 \times 64$	0.0797(3)	0.3143(52)	0.660(7)	2.604(49)	5.79

Table 2
Lattice estimates of r_0/a for different β, extrapolated to the chiral limit [12].

β	5.25	5.29	5.40
r_0/a	6.603(53)	7.004(54)	8.285(74)

for all data sets apart from the more recent analyses at $\beta = 5.29$, $\kappa = 0.13632$ and $\kappa = 0.13640$. For $\kappa = 0.13632$ our aforementioned direct calculation of the σ-term was performed [7], for which a more optimized smearing was critical to obtaining a signal for the scalar matrix element. We achieved this by using Wuppertal smearing with APE smoothed links. This improved method was also applied to our calculations at $\kappa = 0.13640$.

Table 1 lists our data for the pseudoscalar (am_π) and nucleon masses (aM_N). We also state the corresponding values $r_0 m_\pi$ and $r_0 M_N$ in units of the Sommer scale r_0, extrapolated to $m_\ell = 0$ [12] (see Table 2). The error quoted for am_π and aM_N is the statistical uncertainty of the data, while for $r_0 m_\pi$ ($r_0 M_N$) it is the combined error of r_0/a and am_π (aM_N).

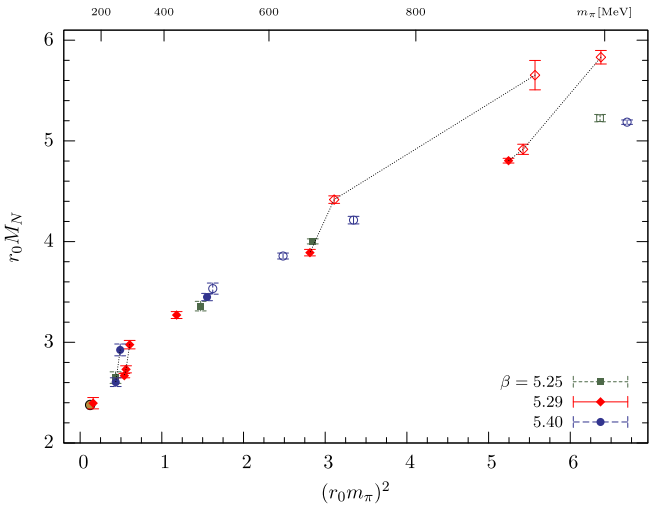

Fig. 1. Lattice data for $r_0 M_N$ versus $(r_0 m_\pi)^2$ for different lattice spacings ($\beta = 5.25$, 5.29, 5.40) and volumes. Open (filled) symbols refer to points where $L \leqslant 3r_0$ ($L > 3r_0$). A black-framed (yellow) circle indicates the physical point assuming $r_0 = 0.5$ fm. The dotted lines connect points of the same (β, κ) but different lattice size. They are meant to guide the eye and to illustrate finite-volume effects. (For interpretation of the references to color in this figure legend, the reader is referred to the web version of this article.)

In Fig. 1 we show our data for $r_0 M_N$ plotted versus $(r_0 m_\pi)^2$. Different symbols and colors are used to distinguish between data for the different β. Data points which refer to the same (β, κ) but different lattice volumes are connected by dotted lines to emphasize finite volume effects.

From this figure (and also from closer inspection of the data) we find that, within the given precision, our data show no systematic dependence on the lattice spacing and, thus, are close to the continuum limit. We therefore scale our data by the respective values of the chirally extrapolated r_0/a and do not attempt a continuum-limit extrapolation. Finite volume effects, on the other hand, are clearly visible and will be incorporated into the fits. In fact, they provide an additional valuable input, because some of the low-energy constants (LECs) also enter the volume corrections.

Before fitting these data to BChPT expressions, all values for the pion mass have to be extrapolated to infinite volume. A method to calculate these finite-volume corrections has been worked out in [13]. When applying this method to our data we find, however, that the corresponding values for $m_\pi L$ have to satisfy at least $m_\pi L > 3.5$. Below this limit, the finite-size effects of our pion mass data are stronger than the calculated corrections. If $m_\pi L \geqslant 4$ the data points and the extrapolated values even agree within errors (see Fig. 2 for an illustration). This means that, within the available precision, correcting for finite-volume effects according to [13] will only help us if $3.5 \leqslant m_\pi L \leqslant 4.0$. In all these cases we have at least one point with $m_\pi L \approx 4$ (or larger).

For the final fits to BChPT, we therefore exclude all (β, κ) combinations for which there is not at least one data point that satisfies $m_\pi L > 3.5$, and then take the value for $r_0 m_\pi$ from the largest available volume (with $m_\pi L > 4$) as our estimate of the infinite-volume limit. As argued above, a finite-volume correction according to Ref. [13] would not give different results for $r_0 m_\pi$, but in this way we are a bit more conservative about the error.

There is, however, one data point where we allow for an exception to this rule: the estimate for $r_0 m_\pi$ at $\beta = 5.29$ and $\kappa = 0.13640$ ($m_\pi \approx 157$ MeV). At these parameters the largest available

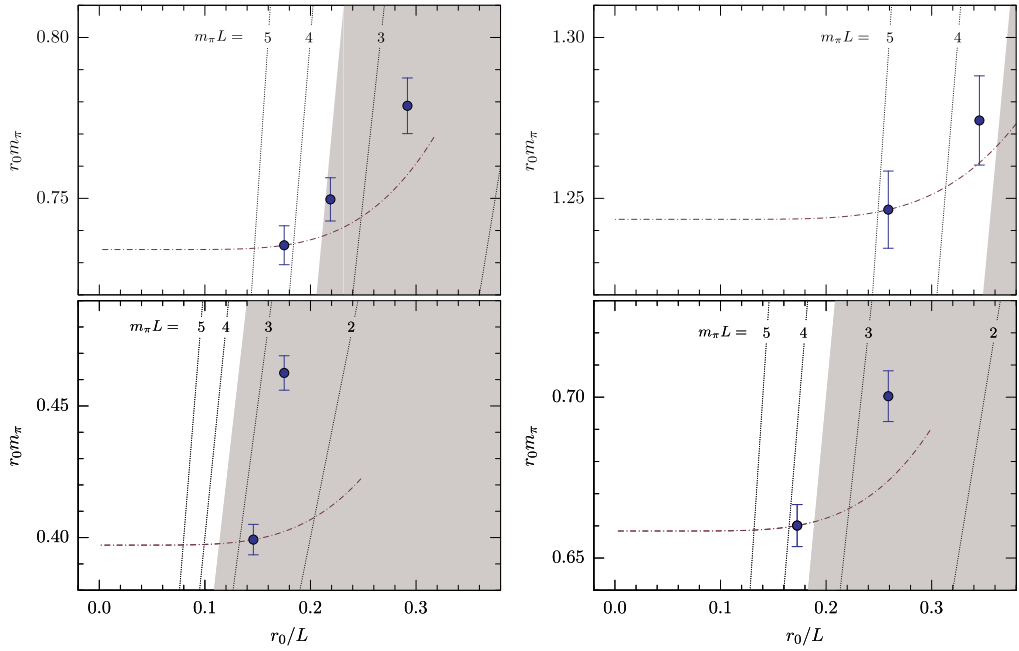

Fig. 2. Volume dependence of our pion mass data. Left top: $\beta = 5.29$, $\kappa = 0.13632$. Left bottom: $\beta = 5.29$, $\kappa = 0.13640$. Right top: $\beta = 5.40$, $\kappa = 0.13640$. Right bottom: $\beta = 5.40$, $\kappa = 0.13660$. Dashed–dotted lines represent finite-volume extrapolations, obtained from applying the method of [13] to the point for the smallest r_0/L. Vertical dotted lines denote constant $m_\pi L$. Gray areas mark the region ($m_\pi L < 3.5$) where finite-volume corrections are not under control.

lattice size is currently $48^3 \times 64$, but we expect no drastic changes of $r_0 m_\pi$ if the volume is enlarged further, because the PCAC-mass dependence of our pion mass data below 290 MeV (considering largest-volume data only) is quite linear already.[1]

As mentioned above, a novel feature of our analysis is that we take additional data for σ into account, which comes from a direct determination. So far, we have computed this at $\beta = 5.29$, $\kappa = 0.13632$ on a $32^3 \times 64$ and $40^3 \times 64$ lattice [7]. This corresponds to a pion mass of about 290 MeV, and we will use the value

$$r_0 \sigma = 0.273(25) \tag{3}$$

from the $40^3 \times 64$ lattice in what follows.

3. Fitting to covariant chiral perturbation theory

3.1. Fitting formulae

We intend to fit our data to BChPT. The expressions at next-to-leading one-loop order are given in Appendix A. We expand those up to order m_π^4:

[1] Note also that if with larger volumes the pion mass further decreased the χ_r^2-value of our fits presented below would actually improve, with negligible effects on the fitted parameters. We have tested that.

$$M_N = M_0 - 4c_1 m_\pi^2 - \frac{3g_A^2 m_\pi^3}{32\pi F_\pi^2} + 4e_1^r m_\pi^4 + \frac{m_\pi^4}{8\pi^2 F_\pi^2}\left[\frac{3c_2}{16} - \frac{3g_A^2}{8M_0} + \log\frac{m_\pi}{\lambda}\left(8c_1 - \frac{3c_2}{4} - 3c_3 - \frac{3g_A^2}{4M_0}\right)\right], \tag{4}$$

$$\sigma = -4c_1 m_\pi^2 - \frac{9g_A^2 m_\pi^3}{64\pi F_\pi^2} + m_\pi^4\left[8e_1^r - \frac{8c_1 l_3^r}{F_\pi^2} + \frac{3c_1}{8\pi^2 F_\pi^2} - \frac{3c_3}{16\pi^2 F_\pi^2} - \frac{9g_A^2}{64\pi^2 M_0 F_\pi^2} + \frac{1}{4\pi^2 F_\pi^2}\log\frac{m_\pi}{\lambda}\left(7c_1 - \frac{3c_2}{4} - 3c_3 - \frac{3g_A^2}{4M_0}\right)\right]. \tag{5}$$

These expressions involve the low-energy constants c_1, c_2 and c_3 as well as the renormalized counterterm coefficient e_1^r and

$$l_3^r \equiv -\frac{1}{64\pi^2}\left(\bar{l}_3 + 2\log\frac{m_\pi^{\text{phys}}}{\lambda}\right), \tag{6}$$

which depend on the renormalization scale λ. The pion decay constant F_π and the nucleon axial coupling constant g_A are taken at the physical point, which is consistent with the order of BChPT we are using. For the fits we will set $F_\pi = 92.4$ MeV and $g_A = 1.256$. The renormalization scale λ is set to $\lambda = m_\pi^{\text{phys}} = 138$ MeV.[2]

To correct for finite-volume effects in our nucleon mass data we employ the finite-volume correction at next-to-leading one-loop order in BChPT. It reads

$$\Delta M_N\left(m_\pi^2, L\right) = \Delta M^{(3)}\left(m_\pi^2, L\right) + \Delta M^{(4)}\left(m_\pi^2, L\right), \tag{7}$$

where $\Delta M^{(3)}$ and $\Delta M^{(4)}$ can be read off from Eqs. (A.15) and (A.16) with the substitution $\overline{m} \to m_\pi$. This is consistent with the order we are using.

Since our data is given in units of r_0, for the fits we have to re-express all dimensionful quantities in units of r_0, too:

$$\begin{aligned} &M_N(m_\pi) \to \widehat{M}_N(\widehat{m}_\pi), \\ &\Delta M_N(m_\pi, L) \to \Delta\widehat{M}_N(\widehat{m}_\pi, \widehat{L}) \quad \text{and} \quad \sigma(m_\pi) \to \widehat{\sigma}(\widehat{m}_\pi) \end{aligned} \tag{8}$$

where a "$\widehat{\ }$" indicates the expression is understood in units of r_0, e.g., $\widehat{M}_N = r_0 M_N$.

As not all parameters of Eqs. (4) and (5) are well constrained by our fits, some of these will be fixed to their phenomenological values, e.g., F_π, c_2, c_3 and $\bar{l}_3$. Consequently, a *physical* input value for r_0 has to be provided as well, which is however unknown a priori.

We fix r_0 for each fit separately by iterating over different physical $r_0^{(k)}$ ($k = 1, 2, \ldots$), plugged into the fitting formulae until r_0 comes out self-consistently from the fit, that is

$$\epsilon > \left|r_0^{(k)} - r_0^{(k-1)}\right| \quad \text{where } r_0^{(k)} = \frac{\widehat{M}_N(r_0^{(k-1)} \cdot m_\pi^{\text{phys}})}{M_N^{\text{phys}}}. \tag{9}$$

We set $\epsilon = 0.001$, and for most of our fits r_0 converges after 10–15 iterations. By construction, all fits will pass through the physical point $M_N^{\text{phys}} = 938$ MeV at $m_\pi^{\text{phys}} = 138$ MeV.

[2] Note that choosing another renormalization scale will only change the values of e_1^r and l_3^r. All other parameters are invariant. We have checked that this is satisfied for our fits.

Two kinds of fits will be discussed below: fits to our nucleon mass data, using the χ^2-function

$$\chi_N^2 = \sum_{i=1}^{N_{\text{data}}} \frac{(\widehat{M}_N(x_i) + \Delta\widehat{M}_N(x_i, y_i) - z_i)^2}{e_i^2} \tag{10}$$

and combined (simultaneous) fits to the nucleon and σ-term data, using the χ^2-function

$$\chi_{N\sigma}^2 = \chi_N^2 + \frac{(\widehat{\sigma}_N(x_j) - \bar{z}_j)^2}{\bar{e}_j^2}. \tag{11}$$

Here $x = r_0 m_\pi$, $y = L/r_0$, $z = r_0 M_N$ refer to our measured points and e denotes the error of $r_0 M_N$. In $\chi_{N\sigma}^2$, $\bar{z}_j$ ($j \in \{1, \ldots, N_{\text{data}}\}$) refers to our single directly determined result for $r_0\sigma$ and $\bar{e}_j$ is its error, see Eq. (3). As finite-size effects appear to be negligible for this number (see Ref. [7]) we do not apply any finite-volume corrections in this case.

3.2. Fit ranges

Our nucleon mass data of Table 1 covers a range of $r_0 m_\pi$ values from 0.42 up to 4.04, and L/r_0 ranges from 1.71 to 6.85. In physical units this corresponds to $m_\pi \approx 0.17$–1.58 GeV and $L = 0.85$–3.4 fm when $r_0 = 0.5$ fm. When fitting these data we do not know a priori for which range of values of m_π and L we can trust our fitting functions. We therefore vary constraints on $r_0 m_\pi$ (L/r_0) from above (below). The constraint $L/r_0 > 3$ turns out to be low enough such that there is sufficient data to perform stable fits but also large enough so that ΔM_N captures the finite-volume effects, see, e.g., the discussion below.

For $r_0 m_\pi$, on the other hand, we find it reasonable to constrain it from above by $(r_0 m_\pi)^2_{\max} = 1.6$, if not $(r_0 m_\pi)^2_{\max} = 1.3$. Both these upper bounds give results which agree within errors, albeit with a larger uncertainty for the latter. Also our independent measurement of $r_0\sigma$ [Eq. (3)] at $r_0 m_\pi \approx 0.735$ is then well reproduced by Eq. (5), not only for a combined fit [Eq. (11)] but also if one uses Eq. (5) with the parameters from a stand-alone fit to the nucleon mass data. For larger $(r_0 m_\pi)^2_{\max}$, say $(r_0 m_\pi)^2_{\max} = 3.0$, the fits change quantitatively and qualitatively: The m_π-dependence of the nucleon mass [Eq. (4)] becomes more concave in shape and our data point for $r_0\sigma$ lies below the fit curves. If one only considered the nucleon mass data, such fits over a larger m_π-range would roughly capture the overall m_π-dependence [even up to $m_\pi \approx 1$ GeV where $O(p^4)$ BChPT certainly does not hold], but this is likely to be accidental for the given order as was pointed out already in [14]. Our definitive analysis will therefore be restricted to fits for which $(r_0 m_\pi)^2_{\max} \leqslant 1.6$. For our final estimates of r_0 and σ we will even restrict ourselves to $(r_0 m_\pi)^2_{\max} \leqslant 1.3$.

3.3. Parameters

Let us now discuss the parameters in the fit functions. Besides F_π and g_A, the functions in Eqs. (10) and (11) contain five and six free parameters, respectively. These are M_0, c_i ($i = 1, 2, 3$) and e_1^r for Eq. (10) and $\bar{l}_3$ in addition for Eq. (11). Ideally one would like to determine these all from fits to the lattice data. This is however not possible with our current data and we therefore have to fix some of the parameters to values from the literature.

As $\bar{l}_3$ only enters $r_0\sigma$ [see Eq. (5)] this parameter should not be left free in a fit with only one data point to constrain it. For our combined fits [Eq. (11)] we therefore fix it to the FLAG-estimate [15]

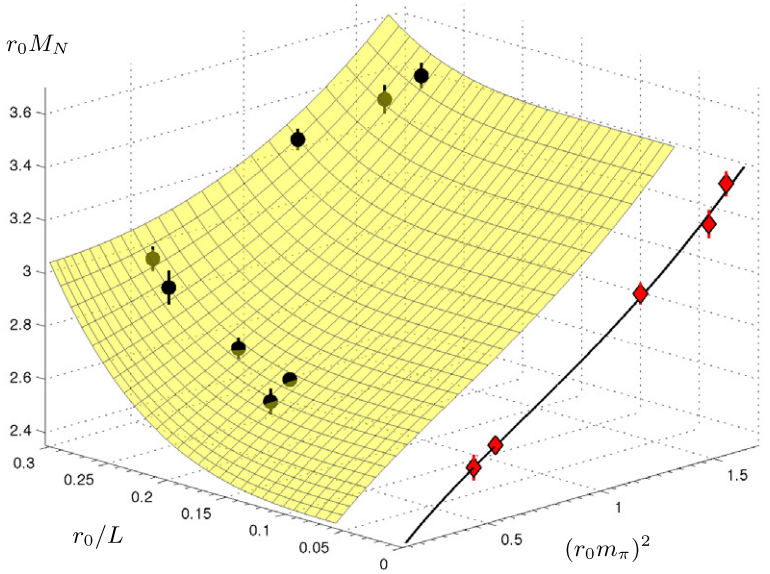

Fig. 3. Fit (surface) to the nucleon mass data (full circles) for a range of r_0/L and $(r_0 m_\pi)^2$ values. Black circles lie above the surface, gray (or half gray) below (or on) the surface. The line and the red diamonds at $r_0/L = 0$ mark the fitted infinite volume prediction. For the sake of simplicity, for each $(r_0 m_\pi)^2$ only one extrapolated (red) point is shown at $r_0/L = 0$. (For interpretation of the references to color in this figure legend, the reader is referred to the web version of this article.)

$$\bar{l}_3 = 3.2(8) \tag{12}$$

and check for the stability of our final results varying $\bar{l}_3 = 3.2$ within one standard deviation.

For c_2 and c_3 we proceed similarly. At first one might be tempted not to fix these two parameters at all. However, like the renormalization-scale dependent parameter e_1^r, c_2 and c_3 gain influence at larger m_π. So, if these parameters are all left free in fits to low m_π-mass data, their uncertainties would be unreasonably large. We therefore decided to fix c_2 and c_3 to their latest phenomenological values [16,17],

$$c_2 = 3.3(2)\ \text{GeV}^{-1} \quad \text{and} \quad c_3 = -4.7(1.3)\ \text{GeV}^{-1}, \tag{13}$$

and investigate the stability of our final results varying the less precisely known parameter c_3 by one standard deviation. Additional fits are performed where c_3 is left as a free parameter.

To check the stability of the fit parameters c_1 and M_0, and also of our estimates of $r_0 M_N^{\text{phys}}$ and $r_0\sigma$ at the physical point, additional fits are performed where the expressions in Eqs. (4) and (5) are truncated at orders $O(m_\pi^3)$ and $O(m_\pi^2)$.

4. Results

4.1. Discussion of our fits

In Fig. 3 we show an example fit to the nucleon mass data. Full (black) circles in Fig. 3 represent our lattice data for the nucleon mass, and the surface is a fit to these points. We fit to the surface $r_0 M_N(r_0 m_\pi, L/r_0)$, hence the finite-volume corrections are determined directly

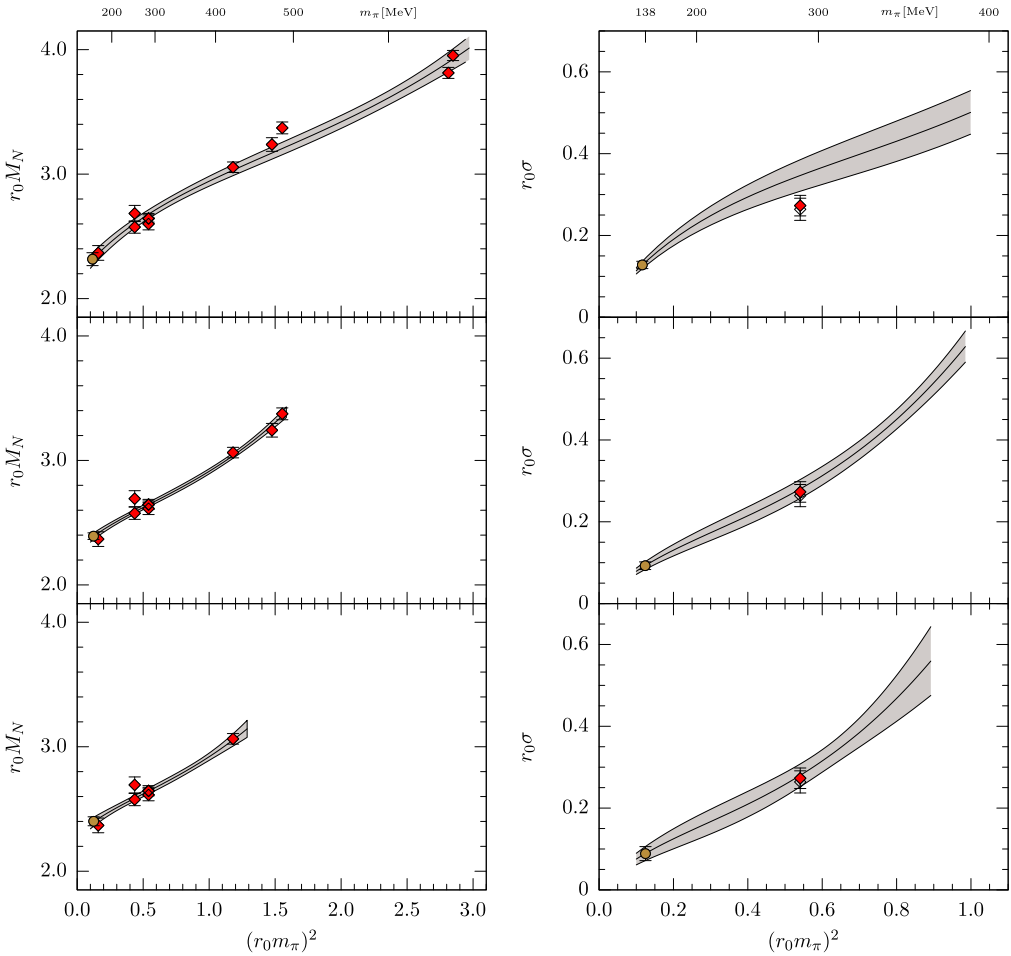

Fig. 4. Simultaneous fits to the nucleon mass (left) and σ-term data (right) for three fitting windows with $(r_0 m_\pi)^2_{\max} = 3.0$, 1.6 and 1.3 (from top to bottom). These fits are labeled `S003`, `S002` and `S001` in Table 4, where $c_2 \equiv 3.3\ \mathrm{GeV}^{-1}$, $c_3 \equiv -4.7\ \mathrm{GeV}^{-1}$ and $\bar{l}_3 \equiv 3.2$. Lines, error bands and (full red) points are shown for the limit $L \to \infty$ (cf. Fig. 3). A black-framed circle marks the location of the physical point using—for each plot separately—the r_0-value for which the fit is self-consistent. Open points did not enter any fit. In the left plots, the overlap of red points at $(r_0 m_\pi)^2 = 0.436$ and 0.538 indicates the quality of the (fitted) finite-volume corrections. (For interpretation of the references to color in this figure legend, the reader is referred to the web version of this article.)

through the fit as well. The (red) diamonds in Fig. 3 represent the lattice data, after subtracting these volume corrections.

An overview of our fits and parameters can be found in Appendix B where we list all our combined and stand-alone fits in Tables 4 and 5, respectively, and also provide more detail for the interested reader.

In Figs. 4 and 5 we display the fit curves corresponding to some of the results listed in these tables, together with the lattice data after subtracting the volume corrections. The overlap of points indicates the quality of these fitted corrections. In Fig. 4, three of our combined fits are

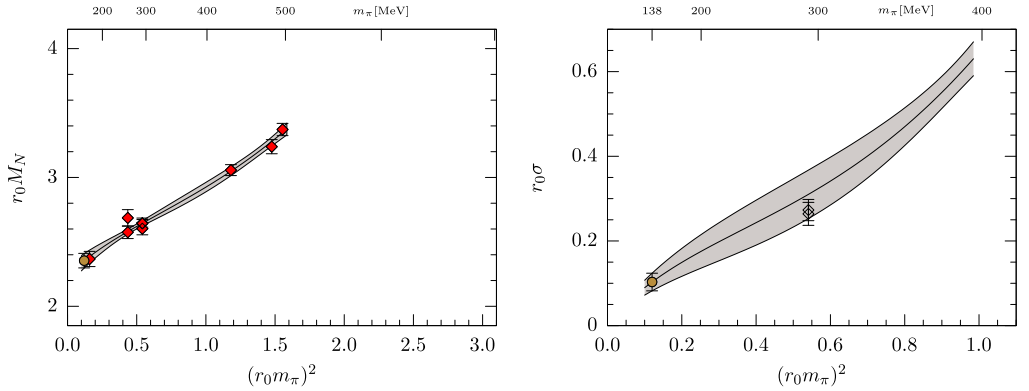

Fig. 5. Left panel: stand-alone fit to the nucleon mass data (see fit No02 in Table 5). Right panel: comparison of the σ-term data (open symbols) for a $32^3 \times 64$ and $40^3 \times 64$ lattice [7] and the BChPT expression for $\sigma(m_\pi)$ with the parameters M_0, c_1 and e_r^1 taken from the nucleon mass fit shown in the left panel. The black-framed circle is the value for $r_0 M_N$ ($r_0\sigma_N$) at the physical point for these parameters. In both panels, the one-sigma error band is shown in gray. As in Fig. 4, the overlap of (red) points (left panel) at same $(r_0 m_\pi)^2$ indicates the quality of the (fitted) finite-volume corrections. (For interpretation of the references to color in this figure legend, the reader is referred to the web version of this article.)

shown (So03, So02 and So01 of Table 4), each for the same choice of fixed parameters (c_2, c_3 and $\bar{l}_3$ as given in Eqs. (12) and (13)), but for different fit ranges

$$(r_0 m_\pi)^2 < (r_0 m_\pi)^2_{\max}, \tag{14}$$

where $(r_0 m_\pi)^2_{\max}$ is 3.0, 1.6 or 1.3, always requiring $L/r_0 > 3$. Fig. 5 shows a corresponding stand-alone fit (No02 of Table 5) to the nucleon mass data for $(r_0 m_\pi)^2_{\max} = 1.6$.

Our fits perform significantly better if the σ-term constraint [Eq. (3)] is incorporated. For these combined fits the individual uncertainty of each fit parameter is smaller than for the corresponding fit to the nucleon mass data alone, while the χ_r^2-values ($\chi_r^2 \equiv \chi^2/ndf$) largely remain unaffected. Fits qualities are inferior, if nucleon mass data up to $(r_0 m_\pi)^2 = 3.0$ is included, but if one lowers this upper bound to 1.6 or 1.3, χ_r^2-values around 1 can be reached. Also the data point for $r_0\sigma$ [Eq. (3)] then agrees with the $O(p^4)$ BChPT expression for $\sigma(m_\pi)$ [Eq. (5)], whether or not the data point for $r_0\sigma$ was included in the fit (compare Figs. 4 and 5). For the fit range $(r_0 m_\pi)^2 < 3.0$ this is not the case anymore.

4.2. Weighted averages

Based on the results summarized in Table 4, we estimate the weighted averages of our fit results for $r_0\sigma_{\text{phys}}$ and $r_0 M_N^{\text{phys}}$. For the weights we use the statistical error, and only values from fits with $\chi_r^2 < 1.3$ are allowed to enter the average. We obtain the values listed in Table 3. As one can see from this table, our results for r_0 for $(r_0 m_\pi)^2 < 1.6$ and $(r_0 m_\pi)^2 < 1.3$ are consistent within errors, including that from the stand-alone fit.

In this table we also give the systematic error due to varying c_3 (second parenthesis) and $\bar{l}_3$ (third parenthesis) one standard deviation around their phenomenological values in Eqs. (12) and (13). In total the systematic error is as large as the statistical error.

Table 3
Weighted averages of fit results with $\chi_r^2 < 1.3$. The first row gives averages for (stand-alone) fits to the nucleon mass data; the remaining rows for (combined) fits to the nucleon mass and σ-term data. The first column specifies the order of the chiral expansion, the second the upper limit on $r_0 m_\pi$. Some of the weighted averages come with a statistical and systematic error: The error in the first parenthesis is always the statistical error and the second (third) the systematic error estimated by changing the fixed parameter c_3 ($\bar{l}_3$) by one standard deviation [see Eq. (12) and (13)]. The numbers that went into the averages are listed in Tables 4 and 5.

Fit	$(r_0 m_\pi)^2_{\max}$	$r_0\sigma_{\text{phys}}$	r_0 [GeV^{-1}]	r_0 [fm]	σ_{phys} [MeV]
$O(m_\pi^4) : \chi_N^2$	1.6	0.103(23)(5)	2.51(6)(2)	0.495(12)(4)	41(9)(2)
$O(m_\pi^4) : \chi_{N\sigma}^2$	1.6	0.095(11)(12)(4)	2.54(3)(4)(2)	0.501(6)(8)(4)	37(4)(5)(2)
$O(m_\pi^4) : \chi_{N\sigma}^2$	1.3	0.093(20)(15)(5)	2.54(5)(5)(2)	0.501(10)(10)(4)	37(8)(6)(2)
$O(m_\pi^3) : \chi_{N\sigma}^2$	1.0	0.121(5)	2.49(3)	0.491(6)	49(2)
$O(m_\pi^2) : \chi_{N\sigma}^2$	1.0	0.065(7)	2.58(3)	0.509(5)	25(3)

4.3. Fits to lower order expansions

It is interesting to check the robustness of the above estimates for r_0 and σ_{phys} by fits to $O(m_\pi^2)$ and $O(m_\pi^3)$ BChPT. Up to these orders, only c_1 and M_0 are left as free parameters. Note that we still have to correct for the finite-volume effect in the nucleon mass data. We do this by setting (as above) $c_2 = 3.3$ GeV^{-1} and $c_3 = -4.7$ GeV^{-1} in ΔM_N.

For the fits to $O(m_\pi^2)$ and $O(m_\pi^3)$ BChPT we employ the χ^2-function for our combined fits [Eq. (11)]. The fitting ranges are chosen as above but we add to these $(r_0 m_\pi)^2_{\max} = 1.0$. It turns out that only for $(r_0 m_\pi)^2_{\max} = 1.0$ reasonable fits to $O(m_\pi^2)$ and $O(m_\pi^3)$ BChPT can be found.

Our results for $r_0\sigma_{\text{phys}}$ and r_0 from these fits are listed in Table 3. To ease the comparison we also show them with our $O(m_\pi^4)$ results in Fig. 6. Open (full) symbols correspond to fits where $\chi_r^2 > 2$ ($\chi_r^2 < 2$), black-framed full symbols represent good fits where $\chi_r^2 < 1.3$.

As can been seen from this figure, fits to different orders in m_π result in slightly different estimates both for r_0 and $r_0\sigma_{\text{phys}}$, and also come with a different fit quality. However, these deviations get smaller when increasing the order or decreasing $(r_0 m_\pi)^2_{\max}$. For fixed $(r_0 m_\pi)^2_{\max}$, points for different orders seem to alternate around a yet unknown value with the tendency of coming closer to that with each order. Results from fits to even larger orders or lower $(r_0 m_\pi)^2_{\max}$ will likely be found within the error bounds of the $O(m_\pi^4)$ results.

We therefore conclude that our estimates for r_0 and σ_{phys}, that is, the weighted averages of our results from the combined $O(m_\pi^4)$ fits with $(r_0 m_\pi)^2_{\max} = 1.3$, lead to sufficiently conservative errors to accommodate all of the uncertainties involved when fitting nucleon mass data to BChPT.

4.4. Comparing different orders

Let us finally try to get an impression of the convergence properties of the BChPT formulae we are using. To this end we plot in Fig. 7 a combined fit (`Sfo1` in Table 4, where c_3 is a free parameter) along with the curves which result from truncating the BChPT function at $O(m_\pi^2)$ and at $O(m_\pi^3)$, using the same parameter values. In addition we show two (three) curves where the contribution of fifth order in m_π has been added to the fitted function varying the new LECs d_{16}^r, d_{18}^r and l_4^r appearing in this contribution within a phenomenologically acceptable (slightly expanded) range. At this order, the LECs d_{16}^r and d_{18}^r enter as the difference $2d_{16}^r - d_{18}^r$ (see Appendix A for details), which currently is known only approximate, $2d_{16}^r - d_{18}^r = (-2.0 \pm 2.5)$ GeV^{-2} [18,19]. For l_4^r we use the value for $\bar{l}_4$ given in [15].

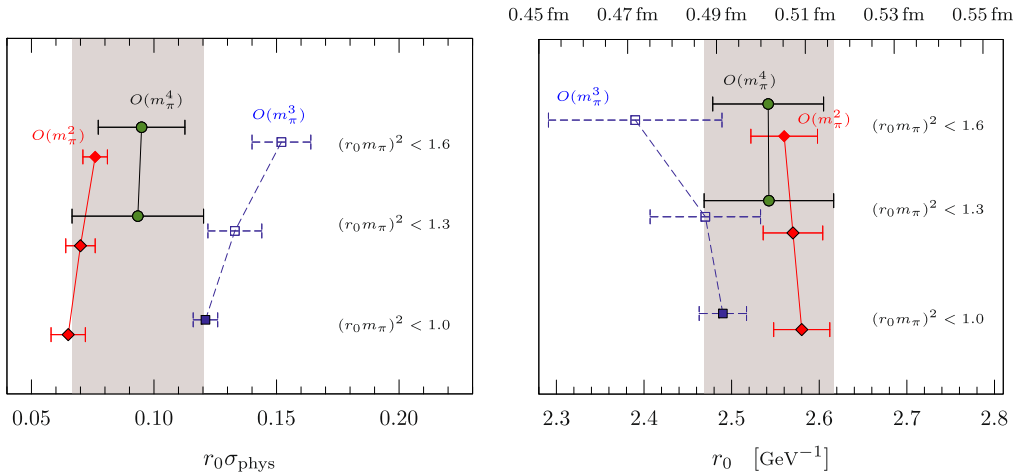

Fig. 6. Results for $r_0\sigma$ at the physical point (left panel) and r_0 (right panel) from fits to BChPT truncating the fit functions $M_N(m_\pi)$ and $\sigma(m_\pi)$ at different orders in m_π. Only results for our combined fits [Eq. (11)] are shown. Points are grouped together with respect to the upper cutoff on $(r_0 m_\pi)^2$. Red diamonds are for fits to order $O(m_\pi^2)$, blue squares are for $O(m_\pi^3)$. Green circles refer to the weighted averages in Table 3, where for the error the statistical and systematic errors have been added in quadrature. Full (open) symbols refer to fits for which $\chi_r^2 < 2.0$ (> 2.0); black-framed full symbols to fits where $\chi_r^2 < 1.3$. The gray bands represent the errors for the lower green circle, which corresponds to our final values for $r_0\sigma_{\rm phys}$ (left) and r_0 (right). (For interpretation of the references to color in this figure legend, the reader is referred to the web version of this article.)

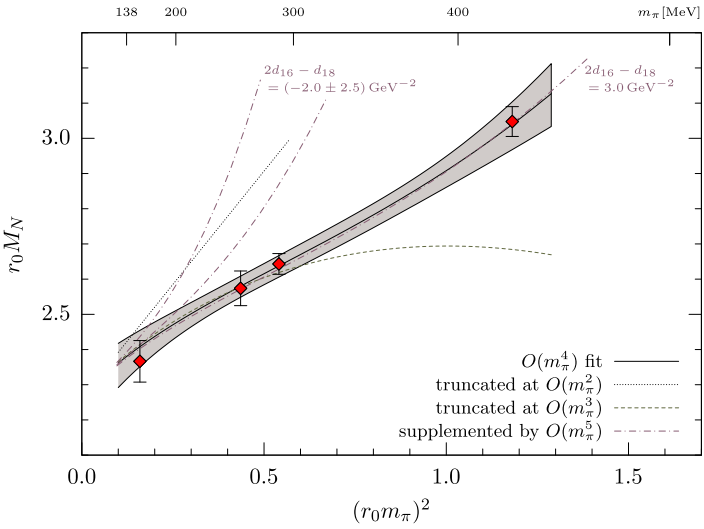

Fig. 7. Comparison of one of our combined fits to the contributions from lower orders ($O(m_\pi^2)$ and $O(m_\pi^3)$) and to the $O(m_\pi^5)$ expansion. For all expansions the parameters are fixed to those of the fit (`Sfo1` in Table 4). The additional parameters for the $O(m_\pi^5)$ expansion were fixed to values consistent with current expectations (see text). In addition, we show the $O(m_\pi^5)$ expansion assuming a larger value for $2d_{16} - d_{18}$ than currently expected from phenomenology (very right dashed–dotted line). For simplicity, we show only finite-volume corrected data (diamonds) from the largest lattice volumes, even though for $(r_0 m_\pi)^2 = 0.435$ and 0.540 also points from smaller volumes entered the fit.

Given this range of expected values, we see that the fifth order correction becomes a non-negligible effect already at pion masses well below the physical kaon mass. More specifically, at pion masses of ~ 350 MeV, the fifth order contribution is already of about the same size as the third order term from the leading-one-loop correction. This leads us to the conclusion that, in case of the nucleon mass and sigma term, BChPT (with the current LECs) shows no sign of convergence beyond $m_\pi > 250$ MeV. Discussions pointing in this direction can also be found in, e.g., [14,20–23]. If one allowed, however, for a slightly wider range for $2d_{16}^r - d_{18}^r$, say $2d_{16}^r - d_{18}^r = 3.0\ \mathrm{GeV}^{-2}$, the fifth order contribution could be much smaller (see Fig. 7). But this is speculative only, and an improved knowledge on the values for d_{16}^r and d_{18}^r is required to decide on that. At least from the small difference of the $O(p^3)$ and $O(p^4)$ functions at small $(r_0 m_\pi)^2$, we learn that the LECs c_2, c_3 and e_1^r are not well constrained by nucleon mass data at pion masses $m_\pi < 300$ MeV.

5. Conclusions

We have presented $N_f = 2$ QCD nucleon mass data. The corresponding pion mass values range from about 1.5 GeV down to 157 MeV. To estimate the nucleon σ-term we have performed two kinds of fits to expressions from $O(p^4)$ BChPT: (stand-alone) fits to our nucleon mass data and simultaneous fits to the nucleon mass and σ-term data. The latter was determined in a separate study [7] at a pion mass of about 290 MeV.

For the fits, different fitting ranges in m_π and L (spatial lattice extension) have been tested. We find that if one demands $m_\pi < 500$ MeV $[(r_0 m_\pi)^2 < 1.6]$ and also $L > 1.5$ fm acceptable fits to $O(p^4)$ BChPT can be found.[3] These fits do not only give a good description of the m_π dependence of the data but also of the finite-volume effects. Generally, our simultaneous fits perform better than fits to the nucleon mass data alone. They are also robust against variations of $(r_0 m_\pi)^2_{\max}$ and of the low energy constants c_2, c_3 and $\bar{l}_3$. We have found a strong correlation between the counterterm coefficient e_1^r and c_3. More data points below 500 MeV pion mass will be needed to resolve this issue or to fix c_2 and c_3 through lattice data.

As our final estimates we quote

$$r_0 = 0.501(10)(11)\ \mathrm{fm} \tag{15}$$

and

$$\sigma_{\mathrm{phys}} = 37(8)(6)\ \mathrm{MeV}. \tag{16}$$

These numbers are the weighted averages given in the last row of Table 3, adding the two systematic errors in quadrature. These numbers result from our fits to $O(p^4)$ BChPT, fitting simultaneously the nucleon mass and σ-term data up to pion masses of about 433 MeV. Within errors, we find these numbers to be consistent with corresponding fits to $O(p^2)$ and $O(p^3)$ BChPT (see Fig. 6), and also with our recent estimate $\sigma_{\mathrm{phys}} = 31(3)(4)$ MeV for $N_f = 2+1$ [9].

Agreement is also found if one compares with other estimates, for example, with the $N_f = 2+1$ estimate of the BMW Collaboration [10], the CSSM results for $N_f = 2$ and $N_f = 2+1$ [11,28,31] or with one of the ETM estimates for $N_f = 2$ [30] (see Fig. 8 for a comparison). Note that ETM quotes a final result $\sigma_{\mathrm{phys}} = 64(1)$ MeV from a fit to $O(p^3)$ BChPT, however they find

[3] Still one needs to have access to m_π-values for which $m_\pi L \geqslant 3.5$. Otherwise the finite-volume effect for m_π is not under control.

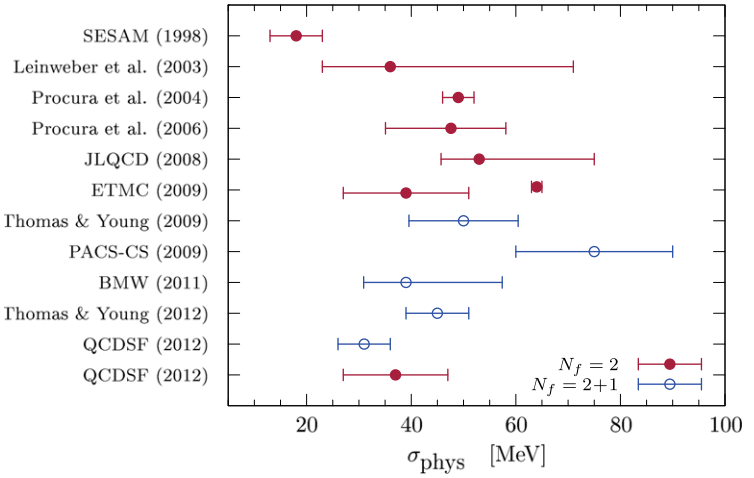

Fig. 8. Comparison of lattice estimates for the pion–nucleon σ-term at the physical point for $N_f = 2$ and $N_f = 2 + 1$ QCD [9,11,24–29]. The lowermost point represents our estimate for $\sigma_{\rm phys}$ [Eq. (16)].

also $\sigma_{\rm phys} = 39(12)$ MeV from a modified fit function (see Figs. 13 and 14 of [30]). Also from our fits to $O(p^3)$ BChPT we could find larger values for σ, depending on the largest pion mass included in the fits. However, based on the systematic procedure we have applied here, we think the value in Eq. (16) is more reliable.

To compare our results with other recent $N_f = 2$ calculations we have redone our combined fits including the raw (i.e., not corrected for finite-size effects) data of the ETM Collaboration [30] into our analysis. This roughly doubles the amount of data which is available at $m_\pi <$ 300 MeV. Repeating fits for different fixed parameter values $\bar{l}_3$, c_2 and c_3 we obtain values for r_0 and $\sigma_{\rm phys}$ which agree within errors with those of Eqs. (15) and (16). The bottom panel of Fig. 9 shows one of these fits: Red diamonds represent our data, blue squares ETMC's points, all after subtracting the finite-volume corrections. As above, these corrections were determined directly through the fit, using points from different volumes but same $(r_0 m_\pi)^2$. For simplicity though, in this figure only points from the largest available lattice volumes are shown. The short (green) band is from the value $r_0\sigma = 0.273(25)$ [7] which constrains the slope of the fitting function at $r_0 m_\pi = 0.735$. The yellow circle marks the physical point using our r_0-value in Eq. (15). For a comparison, the top panel of Fig. 9 shows the corresponding fit (labeled `S001` in Table 4) without ETMC's points included.

We conclude with a note on r_0: The value $r_0 = 0.501(10)(11)$ fm obtained from our fits is somewhat surprising. In other studies (including ours) r_0 was often found to be about 0.47 fm (see, e.g., [30,32–34]). Here r_0 was fixed iteratively forcing the fit to be self-consistent, i.e. $r_0 = \widehat{M}_N(r_0 \cdot m_{\rm phys})/M_N^{\rm phys}$. Our value for r_0 (and that for $\sigma_{\rm phys}$) is thus valid as long as the following assumptions are satisfied: (a) $O(m_\pi^4)$ BChPT is sufficient to describe our data below $m_\pi = 435$ MeV, (b) discretization effects are really negligible and (c) a physical value of 938 MeV is adequate for a two-flavor calculation. Whether these assumptions have to be changed or relaxed has to be seen when there will be more data available at smaller pion masses and lattice spacings, and also for simulations with $N_f = 2 + 1$ and $N_f = 2 + 1 + 1$. From the right panel of Fig. 6, however, we see a trend for r_0: it increases when the upper limit on $r_0 m_\pi$ is lowered.

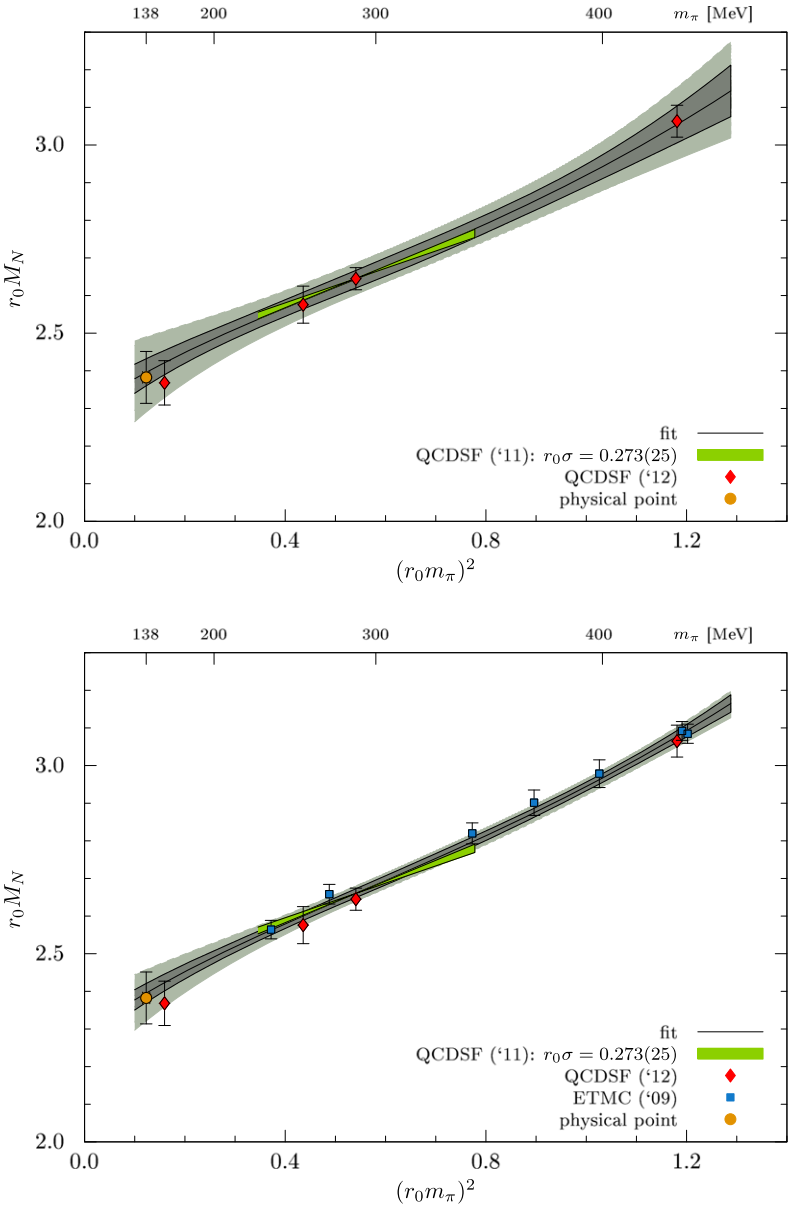

Fig. 9. Top: combined fit to our nucleon mass (red diamonds) and σ-term data (light green band). Shown are the volume-corrected data (determined through the fit) for one volume only. The fit's characteristics (fit ranges, fixed parameters) are the same as for the fit labeled `S001` in Table 4. The inner band is the error band for the fit, the outer band illustrates the variation of the fit changing $\bar{l}_3$ and c_3 by one standard deviations around their phenomenological values [Eqs. (12) and (13)]. For the physical point, marked by a (yellow) circle, we use our final estimate for r_0 [Eq. (15)]. Bottom: same as top panel, but the combined fit also includes the nucleon mass data of the ETM Collaboration (blue squares) [30]. Note that their data is plotted against the π^+ mass. (For interpretation of the references to color in this figure legend, the reader is referred to the web version of this article.)

Note that also a recent study [35] of the kaon decay constant finds a r_0-value of around 0.5 fm from a two-flavor lattice calculation. Their estimate is completely consistent with our estimate of Eq. (15).

Acknowledgements

This work was supported by the European Union under the Grant Agreement numbers 238353 (ITN STRONGnet), 256594 (IRG), 283286 (Hadron Physics 3), and by the Deutsche Forschungsgemeinschaft SFB/Transregio 55. S. Collins acknowledges support from the Claussen-Simon-Foundation (Stifterverband für die Deutsche Wissenschaft). J. Zanotti was supported by the Australian Research Council under grant FT100100005. B Gläßle and N. Najjar received support from the EU Research Infrastructure Action HPC-Europa2 228398. Computations were performed on the SFB/TR55 QPACE supercomputers, the BlueGene/P (JuGene) and the Nehalem Cluster (JuRoPA) of the Jülich Supercomputer Center, the IBM BlueGene/L at the EPCC (Edinburgh) and the SGI Altix ICE machines at HLRN (Berlin/Hannover). We thank the support staffs of these institutions. The Chroma software suite [36] and BAGEL [37] was used in this work and gauge configurations were generated using the BQCD code [38] on QPACE and BlueGenes.

Appendix A. Nucleon mass and pion–nucleon σ-term from BChPT

In this appendix we derive our fit formulae from a next-to-leading one-loop order (or $\mathcal{O}(p^4)$) calculation of the nucleon mass in covariant baryon chiral perturbation theory (BChPT) for two light flavors. The pion–nucleon σ term then follows from an application of the Feynman–Hellmann theorem (see Eq. (2)). In addition we need to know the connection between the quark mass and the pion mass to $\mathcal{O}(p^4)$ [39,40]. Denoting the mass of the degenerate light quarks by $m_\ell = m_u = m_d$ the leading term is given by the Gell-Mann–Oakes–Renner relation

$$m_\pi^2 = 2B_0 m_\ell. \tag{A.1}$$

While the quark mass m_ℓ and the parameter B_0 are scheme and scale dependent, the auxiliary variable

$$\overline{m}^2 \equiv 2B_0 m_\ell \tag{A.2}$$

is independent of these conventions.

The generic $\mathcal{O}(p^4)$ result for the nucleon mass can be written as

$$M_N = M_0 + M^{(1)} + M^{(2)} + M^{(3)} + M^{(4)} + \mathcal{O}\big(p^5\big). \tag{A.3}$$

Evaluating the required loop diagrams with $\overline{\text{IR}}$-regularization [41] one obtains

$$M^{(1)} = 0, \tag{A.4}$$

$$M^{(2)} = -4c_1\overline{m}^2, \tag{A.5}$$

$$M^{(3)} = -\frac{3(g_A^0)^2\overline{m}^3}{16\pi^2(F_\pi^0)^2}\left\{\sqrt{1-\frac{\overline{m}^2}{4M_0^2}}\arccos\frac{\overline{m}}{2M_0} + \frac{\overline{m}}{4M_0}\log\frac{\overline{m}^2}{M_0^2}\right\}, \tag{A.6}$$

$$M^{(4)} = 4\tilde{e}_1^r(\lambda)\overline{m}^4 + \frac{3\overline{m}^4}{64\pi^2(F_\pi^0)^2}\log\frac{\overline{m}^2}{\lambda^2}\left\{8c_1 - c_2 - 4c_3 - \frac{(g_A^0)^2}{M_0}\right\}$$

$$+\frac{3\overline{m}^4}{64\pi^2(F_\pi^0)^2}\left\{\frac{c_2}{2}-3\frac{(g_A^0)^2}{M_0}+\frac{(g_A^0)^2}{M_0}\log\frac{\overline{m}^2}{M_0^2}\right\}$$
$$-\frac{3c_1(g_A^0)^2\overline{m}^6}{16\pi^2(F_\pi^0)^2M_0^2}\left\{\log\frac{\overline{m}^2}{M_0^2}-\frac{\overline{m}}{M_0}\frac{\arccos\frac{\overline{m}}{2M_0}}{\sqrt{1-\frac{\overline{m}^2}{4M_0^2}}}\right\}. \tag{A.7}$$

Here g_A^0 and F_π^0 denote the axial coupling constant of the nucleon and the pion decay constant in the chiral limit, and c_1, c_2, c_3 are the standard low-energy constants (see, e.g., [42]). The renormalized counterterm coefficient $\tilde{e}_1^r(\lambda)$ depends on the scale λ of dimensional regularization in such a way that $M^{(4)}$ does not depend on λ.

The generic next-to-leading one-loop result for the sigma term of the nucleon reads

$$\sigma=\sigma^{(1)}+\sigma^{(2)}+\sigma^{(3)}+\sigma^{(4)}+\mathcal{O}\big(p^5\big). \tag{A.8}$$

Utilizing the relation

$$\sigma=m_\ell\frac{\partial M_N(m_\ell)}{\partial m_\ell}=\overline{m}^2\frac{\partial M_N(\overline{m}^2)}{\partial\overline{m}^2} \tag{A.9}$$

one obtains from Eqs. (A.4)–(A.7)

$$\sigma^{(1)}=0, \tag{A.10}$$
$$\sigma^{(2)}=-4c_1\overline{m}^2, \tag{A.11}$$
$$\sigma^{(3)}=-\frac{3(g_A^0)^2\,\overline{m}^3}{16\pi^2(F_\pi^0)^2}\left\{\frac{3-\frac{\overline{m}^2}{M_0^2}}{2\sqrt{1-\frac{\overline{m}^2}{4M_0^2}}}\arccos\frac{\overline{m}}{2M_0}+\frac{\overline{m}}{2M_0}\log\frac{\overline{m}^2}{M_0^2}\right\}, \tag{A.12}$$
$$\sigma^{(4)}=8\tilde{e}_1^r(\lambda)\overline{m}^4+\frac{3\overline{m}^4}{32\pi^2(F_\pi^0)^2}\log\frac{\overline{m}^2}{\lambda^2}\left\{8c_1-c_2-4c_3-\frac{(g_A^0)^2}{M_0}\right\}$$
$$+\frac{3\overline{m}^4}{32\pi^2(F_\pi^0)^2}\left\{4c_1-2c_3-3\frac{(g_A^0)^2}{M_0}+\frac{(g_A^0)^2}{M_0}\log\frac{\overline{m}^2}{M_0^2}\right\}$$
$$-\frac{3c_1\,(g_A^0)^2\,\overline{m}^6}{16\pi^2(F_\pi^0)^2M_0^2}\left\{\frac{1}{1-\frac{\overline{m}^2}{4M_0^2}}+3\log\frac{\overline{m}^2}{M_0^2}-\left(\frac{7}{2}-\frac{3\overline{m}^2}{4M_0^2}\right)\frac{\overline{m}}{M_0}\frac{\arccos\frac{\overline{m}}{2M_0}}{(1-\frac{\overline{m}^2}{4M_0^2})^{3/2}}\right\}. \tag{A.13}$$

Finite volume corrections to the nucleon mass can be evaluated from the same Feynman diagrams. At next-to-leading one-loop order one gets [43]

$$\Delta M_N\big(\overline{m}^2,L\big)=\Delta M^{(3)}\big(\overline{m}^2,L\big)+\Delta M^{(4)}\big(\overline{m}^2,L\big)+\mathcal{O}\big(p^5\big) \tag{A.14}$$

with

$$\Delta M^{(3)}=\frac{3(g_A^0)^2M_0\overline{m}^2}{16\pi^2(F_\pi^0)^2}\int_0^\infty dx\sum_{\vec{n}\neq\vec{0}}K_0\Big(L|\vec{n}|\sqrt{M_0^2x^2+\overline{m}^2(1-x)}\Big), \tag{A.15}$$

$$\Delta M^{(4)}=\frac{3\overline{m}^4}{4\pi^2(F_\pi^0)^2}\sum_{\vec{n}\neq\vec{0}}\left[(2c_1-c_3)\frac{K_1(L|\vec{n}|\overline{m})}{L|\vec{n}|\overline{m}}+c_2\frac{K_2(L|\vec{n}|\overline{m})}{(L|\vec{n}|\overline{m})^2}\right], \tag{A.16}$$

where K_i is a modified Bessel function. Note that the value $\vec{n} = \vec{0}$ is omitted in the threefold sum over the integers n_1, n_2, n_3.

For the applications in the present paper it is advantageous to consider the nucleon mass as a function of the pion mass m_π (the mass of the lowest lying 0^- state in the simulation). Therefore we have to convert our expressions for $M_N(\overline{m}^2)$ of Eq. (A.3) into expressions for $M_N(m_\pi^2)$. Utilizing the $\mathcal{O}(p^4)$ result [39]

$$m_\pi^2 = \overline{m}^2 + 2l_3^r(\lambda)\frac{\overline{m}^4}{(F_\pi^0)^2} + \frac{\overline{m}^4}{32\pi^2(F_\pi^0)^2}\log\frac{\overline{m}^2}{\lambda^2} + \mathcal{O}\big(p^6\big) \tag{A.17}$$

we can eliminate the dependence on $\overline{m}$ at the cost of introducing the renormalized low-energy constant $l_3^r(\lambda)$, which cancels the dependence on the renormalization scale λ of the associated chiral logarithm in Eq. (A.17). Note, however, that $l_3^r(\lambda)$ can be subsumed into an effective coupling $e_1^r(\lambda)$ via

$$e_1^r(\lambda) \equiv \tilde{e}_1^r(\lambda) + 2l_3^r(\lambda)\frac{c_1}{(F_\pi^0)^2} \tag{A.18}$$

and therefore cannot be determined independently within an analysis of the mass of the nucleon. One finds

$$\begin{aligned} M_N(m_\pi) = {} & M_0 - 4c_1 m_\pi^2 - \frac{3g_A^2 m_\pi^3}{16\pi^2 F_\pi^2}\left\{\sqrt{1-\frac{m_\pi^2}{4M_0^2}}\arccos\frac{m_\pi}{2M_0} + \frac{m_\pi}{4M_0}\log\frac{m_\pi^2}{M_0^2}\right\} \\ & + 4e_1^r(\lambda)m_\pi^4 + \frac{3m_\pi^4}{64\pi^2 F_\pi^2}\log\frac{m_\pi^2}{\lambda^2}\left\{\frac{32}{3}c_1 - c_2 - 4c_3 - \frac{g_A^2}{M_0}\right\} \\ & + \frac{3m_\pi^4}{64\pi^2 F_\pi^2}\left\{\frac{c_2}{2} - 3\frac{g_A^2}{M_0} + \frac{g_A^2}{M_0}\log\frac{m_\pi^2}{M_0^2}\right\} \\ & - \frac{3c_1 g_A^2 m_\pi^6}{16\pi^2 F_\pi^2 M_0^2}\left\{\log\frac{m_\pi^2}{M_0^2} - \frac{m_\pi}{M_0}\frac{\arccos\frac{m_\pi}{2M_0}}{\sqrt{1-\frac{m_\pi^2}{4M_0^2}}}\right\} + \delta M_N^{(5)}. \end{aligned} \tag{A.19}$$

Note that we have shifted the couplings $g_A^0 \to g_A$, $F_\pi^0 \to F_\pi$ to their physical values, consistent to the order at which we are working. This applies also to the finite volume corrections, where we may in addition replace $\overline{m}$ by m_π.

For the σ term as a function of m_π we obtain

$$\begin{aligned} \sigma(m_\pi) = {} & -4c_1 m_\pi^2 - \frac{3g_A^2 m_\pi^3}{16\pi^2 F_\pi^2}\left\{\frac{3-\frac{m_\pi^2}{M_0^2}}{2\sqrt{1-\frac{m_\pi^2}{4M_0^2}}}\arccos\frac{m_\pi}{2M_0} + \frac{m_\pi}{2M_0}\log\frac{m_\pi^2}{M_0^2}\right\} \\ & + 8e_1^r(\lambda)m_\pi^4 - \frac{8c_1 l_3^r(\lambda)}{F_\pi^2}m_\pi^4 + \frac{3m_\pi^4}{32\pi^2 F_\pi^2}\log\frac{m_\pi^2}{\lambda^2}\left\{\frac{28}{3}c_1 - c_2 - 4c_3 - \frac{g_A^2}{M_0}\right\} \\ & + \frac{3m_\pi^4}{32\pi^2 F_\pi^2}\left\{4c_1 - 2c_3 - 3\frac{g_A^2}{M_0} + \frac{g_A^2}{M_0}\log\frac{m_\pi^2}{M_0^2}\right\} \end{aligned}$$

$$- \frac{3c_1 g_A^2 m_\pi^6}{16\pi^2 F_\pi^2 M_0^2}\left\{\frac{1}{1-\frac{m_\pi^2}{4M_0^2}} + 3\log\frac{m_\pi^2}{M_0^2} - \left(\frac{7}{2} - \frac{3m_\pi^2}{4M_0^2}\right)\frac{m_\pi}{M_0}\frac{\arccos\frac{m_\pi}{2M_0}}{(1-\frac{m_\pi^2}{4M_0^2})^{3/2}}\right\}$$
$$+ \frac{5}{2}\delta M_N^{(5)}. \tag{A.20}$$

Note that in contrast to the chiral extrapolation function of the mass of a nucleon given in Eq. (A.19) the dependence on the counter term $l_3^r(\lambda)$ introduced in Eq. (A.17) cannot be absorbed completely into the effective coupling $e_1^r(\lambda)$. In order to calculate $\sigma(m_\pi^{\text{phys}})$ we therefore also need information on the numerical size of the coupling $\bar{l}_3$, which is related to the scale-dependent coupling $l_3^r(\lambda)$ via

$$l_3^r(\lambda) = -\frac{1}{64\pi^2}\left(\bar{l}_3 + \log\frac{\overline{m}^2}{\lambda^2}\right). \tag{A.21}$$

Finally, expanding the expressions for $M_N(m_\pi)$ and $\sigma(m_\pi)$ given in Eqs. (A.19) and (A.20), respectively, in powers of m_π up to $\mathcal{O}(m_\pi^4)$ we arrive at the formulae Eqs. (4) and (5) used in our fits.

Let us now estimate the theoretical uncertainty associated with our next-to-leading one-loop BChPT calculation of M_N due to the truncation of $\mathcal{O}(p^5)$ effects (and all higher orders). A complete two-loop calculation of the nucleon mass in BChPT, employing a reformulated version of infrared regularization, has been worked out in Refs. [23,44]. Truncating the result at $\mathcal{O}(m_\pi^5)$, we find

$$M_N = M_0 + \tilde{k}_1 m_\pi^2 + \tilde{k}_2 m_\pi^3 + \tilde{k}_3 m_\pi^4 \log\left(\frac{m_\pi}{\lambda}\right)$$
$$+ \tilde{k}_4 m_\pi^4 + \tilde{k}_5 m_\pi^5 \log\left(\frac{m_\pi}{\lambda}\right) + \tilde{k}_6 m_\pi^5 + \mathcal{O}\big(m_\pi^6\big). \tag{A.22}$$

The coefficients of this expansion are given by

$$\tilde{k}_1 = -4c_1, \qquad \tilde{k}_2 = -\frac{3(g_A^0)^2}{32\pi(F_\pi^0)^2},$$
$$\tilde{k}_3 = -\frac{3(g_A^0)^2 - 32c_1 M_0 + 3c_2 M_0 + 12c_3 M_0}{32M_0\pi^2(F_\pi^0)^2},$$
$$\tilde{k}_4 = 4e_1^r - \frac{3(2(g_A^0)^2 - c_2 M_0)}{128M_0\pi^2(F_\pi^0)^2}, \qquad \tilde{k}_5 = \frac{3(g_A^0)^4}{64\pi^3(F_\pi^0)^4},$$
$$\tilde{k}_6 = \frac{3g_A^0}{256M_0^2\pi^3(F_\pi^0)^4}\big((g_A^0)^3 M_0^2 + \pi^2\big(16g_A^0 M_0^2 l_4^r + \big(F_\pi^0\big)^2\big(g_A^0 - 32M_0^2\big(2d_{16}^r - d_{18}^r\big)\big)\big)\big).$$

The one-loop expression (coefficients $\tilde{k}_1 - \tilde{k}_4$) is consistent with Eq. (4). In order to study the higher order effects we need values of the additional low-energy constants l_4^r and $2d_{16}^r - d_{18}^r$. From [15,18,19] we find $l_4^r(\lambda = 0.138\ \text{GeV}) = 0.027$ and (with a considerable uncertainty) $d_{16}^r(\lambda = 0.138\ \text{GeV}) = -1.76\ \text{GeV}^{-2}$. For the scale-independent constant d_{18}^r, Ref. [42] derives the value $d_{18}^r = -0.80\ \text{GeV}^{-2}$ from the Goldberger–Treiman relation. In view of the large uncertainty of d_{16}^r we use the rough estimate $2d_{16}^r - d_{18}^r = (-2.5 \pm 2.0)\ \text{GeV}^{-2}$. This estimate, however, does not reproduce the m_π-dependence of our nucleon mass data. Using

$2d_{16}^r - d_{18}^r = 3.0\ \mathrm{GeV}^{-2}$ instead results in much better fits to the data. The $O(m_\pi^5)$ curves in Fig. 7 have been calculated with both these numbers.

The corresponding expansion of the σ term is calculated from the derivative of M_N with respect to the light quark mass according to Eq. (2). Expressed in terms of m_π it reads

$$\sigma = \tilde{h}_1 m_\pi^2 + \tilde{h}_2 m_\pi^3 + \tilde{h}_3 m_\pi^4 \log\left(\frac{m_\pi}{\lambda}\right) + \tilde{h}_4 m_\pi^4 + \tilde{h}_5 m_\pi^5 \log\left(\frac{m_\pi}{\lambda}\right) + \tilde{h}_6 m_\pi^5 + \mathcal{O}\big(m_\pi^6\big), \tag{A.23}$$

with the coefficients

$$\begin{aligned}
\tilde{h}_1 &= -4c_1, \qquad \tilde{h}_2 = -\frac{9(g_A^0)^2}{64\pi(F_\pi^0)^2},\\
\tilde{h}_3 &= -\frac{3(g_A^0)^2 - 28M_0c_1 + 3M_0c_2 + 12M_0c_3}{16M_0\pi^2(F_\pi^0)^2},\\
\tilde{h}_4 &= 8e_1^r - \frac{8c_1 l_3^r}{(F_\pi^0)^2} - \frac{3}{64M_0\pi^2(F_\pi^0)^2}\big(3\big(g_A^0\big)^2 - 8M_0c_1 + 4M_0c_3\big),\\
\tilde{h}_5 &= \frac{3(g_A^0)^2(40(g_A^0)^2 - 3)}{1024\pi^3(F_\pi^0)^4},\\
\tilde{h}_6 &= \frac{3g_A^0}{2048M_0^2\pi^3(F_\pi^0)^4}\big\{3g_A^0\big(12\big(g_A^0\big)^2 - 1\big)M_0^2\\
&\quad + 4\pi^2\big[16g_A^0\big(5l_4^r - 3l_3^r\big)M_0^2 + 5\big(F_\pi^0\big)^2\big(g_A^0 - 32M_0^2\big(2d_{16}^r - d_{18}^r\big)\big)\big]\big\}.
\end{aligned}$$

Finally, we add a remark concerning the LEC e_1^r. Becher and Leutwyler give an estimate for the Delta contribution to $\bar{e}_1^{BL}$ (see Appendix D of [45]):

$$\bar{e}_{1,\Delta}^{BL} = -\frac{g_\Delta^2}{48\pi^2\Delta}\left(6\log\left(\frac{\Delta}{2M_0}\right) + 5\right). \tag{A.24}$$

For $g_\Delta = 13.0\ \mathrm{GeV}^{-1}$, $\Delta = (1.232 - 0.939)$ GeV, this amounts to $\bar{e}_{1,\Delta}^{BL} \sim 7.5\ \mathrm{GeV}^{-3}$. Translated to our choice of LECs, this would give

$$\begin{aligned}
4\tilde{e}_1^r(\lambda = M_N) = {}& 4\bar{e}_1 + \frac{3(g^2 - 8c_1M_0 + c_2M_0 + 4c_3M_0)}{32M_0\pi^2(F_\pi^0)^2}\log\left(\frac{m_{\mathrm{phys}}}{M_N^{\mathrm{phys}}}\right) = 7.5\ \mathrm{GeV}^{-3}\\
&\Rightarrow -1\ \mathrm{GeV}^{-3} \lesssim e_1^r(\lambda = 0.138\ \mathrm{GeV}) \lesssim 1\ \mathrm{GeV}^{-3},
\end{aligned} \tag{A.25}$$

so this (shifted) LEC may therefore be expected to be of natural size. Such resonance saturation estimates usually give only very rough estimates for the higher-order LECs, at least in the baryonic sector. Nonetheless, such a range of values for e_1^r would be consistent with the findings of our fits (cf. Appendix B).

Appendix B. More details on the fits

Here we give a short summary and discussion of the fit parameters for our (simultaneous) fits to the nucleon mass (and σ-term) data. For both types, fits have been performed for different fit ranges and fixed input parameters, c_2, c_3 and $\bar{l}_3$, in order to systematically explore the dependence

Table 4
Parameters from our combined fits to the nucleon mass and σ-term data. Keys in the first column indicate the features of the fits. All keys start with `S..` indicating that the σ-term data has been included when fitting. Entries are ordered according to increasing $(r_0 m_\pi)^2_{\max}$, as specified in column 2. The χ^2-value together with the number of degrees of freedom (ndf) is given in column 3. Columns 4 to 8 list the fit parameters M_0, c_1, e_1^r(0.138 MeV), c_2 and c_3 in units of r_0. The corresponding estimates for $r_0\sigma$ at the physical point and for r_0 are given in column 9 and 10. Since r_0 is not a fit parameter, but has been iteratively fixed as explained in the text, the error for r_0 is that of $\widehat{M}_N(r_0 \cdot m_\pi^{\text{phys}})/M_N^{\text{phys}}$. Lines tagged with a $\star$ indicate fits where $\chi^2/ndf < 1.3$. Parameters of these fits enter the weighted averages given in the lines starting with "ave.".

Key	$(r_0 m_\pi)^2_{\max}$	χ^2_r	$r_0 M_0$	c_1/r_0	e_1^r/r_0^3	c_2/r_0	c_3/r_0	$r_0\sigma_{\text{phys}}$	r_0 [1/GeV]
⋆ `Smm1`	1.30	4.470 / 5	2.26(4)	−0.34(3)	−0.142(11)	1.30	−2.37	0.098(17)	2.53(4)
⋆ `Smo1`	1.30	4.450 / 5	2.22(4)	−0.36(3)	−0.148(10)	1.32	−2.39	0.104(17)	2.51(4)
⋆ `Smp1`	1.30	4.810 / 5	2.19(4)	−0.39(3)	−0.155(10)	1.33	−2.42	0.111(18)	2.48(4)
⋆ `Som1`	1.30	4.550 / 5	2.31(4)	−0.28(3)	−0.022(11)	1.28	−1.83	0.084(18)	2.57(4)
⋆ `Soo1`	1.30	4.060 / 5	2.29(4)	−0.29(3)	−0.024(11)	1.29	−1.84	0.089(17)	2.56(4)
⋆ `Sop1`	1.30	3.690 / 5	2.26(4)	−0.31(3)	−0.027(10)	1.30	−1.85	0.094(17)	2.53(4)
`Spm1`	1.30	6.990 / 5	2.37(4)	−0.22(3)	0.087(12)	1.26	−1.30	0.070(22)	2.61(5)
⋆ `Spo1`	1.30	6.380 / 5	2.35(4)	−0.23(3)	0.087(11)	1.27	−1.31	0.074(22)	2.60(5)
⋆ `Spp1`	1.30	5.770 / 5	2.33(4)	−0.25(3)	0.087(11)	1.28	−1.32	0.079(22)	2.58(5)
ave.	1.30	$\chi^2_r < 1.3$	2.28(4)	−0.31(3)	−0.048(11)	–	–	0.093(18)	2.54(4)
⋆ `Sfm1`	1.30	4.180 / 4	2.28(7)	−0.31(7)	−0.089(127)	1.29	−2.13(58)	0.092(30)	2.55(7)
⋆ `Sfo1`	1.30	3.850 / 4	2.26(7)	−0.32(7)	−0.073(125)	1.30	−2.06(56)	0.095(30)	2.54(7)
⋆ `Sfp1`	1.30	3.620 / 4	2.25(8)	−0.33(7)	−0.054(122)	1.31	−1.98(55)	0.098(30)	2.52(7)
ave.	1.30	$\chi^2_r < 1.3$	2.26(7)	−0.32(7)	−0.072(125)	–	−2.05(56)	0.095(3)	2.54(7)
⋆ `Smm2`	1.60	5.140 / 7	2.25(3)	−0.35(2)	−0.146(5)	1.30	−2.37	0.100(9)	2.53(3)
⋆ `Smo2`	1.60	5.100 / 7	2.22(3)	−0.36(2)	−0.150(5)	1.32	−2.39	0.105(9)	2.51(3)
⋆ `Smp2`	1.60	5.460 / 7	2.19(4)	−0.38(2)	−0.154(5)	1.33	−2.42	0.110(10)	2.48(3)
⋆ `Som2`	1.60	5.270 / 7	2.30(3)	−0.29(2)	−0.028(5)	1.29	−1.83	0.089(10)	2.56(3)
⋆ `Soo2`	1.60	4.730 / 7	2.28(3)	−0.31(2)	−0.029(5)	1.30	−1.84	0.093(9)	2.55(3)
⋆ `Sop2`	1.60	4.350 / 7	2.25(4)	−0.32(2)	−0.030(5)	1.30	−1.86	0.097(9)	2.53(3)
⋆ `Spm2`	1.60	7.820 / 7	2.35(3)	−0.24(2)	0.079(5)	1.27	−1.31	0.078(12)	2.60(4)
⋆ `Spo2`	1.60	7.100 / 7	2.33(3)	−0.25(2)	0.080(5)	1.28	−1.32	0.081(12)	2.59(4)
⋆ `Spp2`	1.60	6.430 / 7	2.31(4)	−0.26(2)	0.081(5)	1.28	−1.32	0.084(11)	2.57(3)
ave.	1.60	$\chi^2_r < 1.3$	2.28(4)	−0.31(2)	−0.033(5)	–	–	0.095(10)	2.54(3)
⋆ `Sfm2`	1.60	4.870 / 6	2.27(6)	−0.32(6)	−0.095(123)	1.30	−2.15(57)	0.096(18)	2.54(5)
⋆ `Sfo2`	1.60	4.510 / 6	2.26(6)	−0.33(6)	−0.077(121)	1.30	−2.07(55)	0.098(18)	2.53(5)
⋆ `Sfp2`	1.60	4.280 / 6	2.24(6)	−0.33(6)	−0.055(118)	1.31	−1.97(54)	0.099(18)	2.52(5)
ave.	1.60	$\chi^2_r < 1.3$	2.26(6)	−0.33(6)	−0.08(12)	–	−2.1(6)	0.098(18)	2.53(5)
`Smm3`	3.00	50.650 / 9	2.11(3)	−0.48(1)	−0.178(5)	1.36	−2.47	0.144(11)	2.43(7)
`Smo3`	3.00	44.340 / 9	2.08(3)	−0.49(1)	−0.180(5)	1.38	−2.50	0.145(10)	2.40(7)
`Smp3`	3.00	38.890 / 9	2.05(3)	−0.51(1)	−0.182(6)	1.39	−2.53	0.146(9)	2.37(6)
`Som3`	3.00	36.360 / 9	2.18(3)	−0.40(1)	−0.045(5)	1.33	−1.89	0.127(10)	2.49(6)
`Soo3`	3.00	31.150 / 9	2.16(3)	−0.40(1)	−0.043(5)	1.34	−1.91	0.128(9)	2.47(6)
`Sop3`	3.00	26.420 / 9	2.14(3)	−0.41(1)	−0.041(5)	1.35	−1.92	0.129(8)	2.45(5)
`Spm3`	3.00	29.170 / 9	2.25(3)	−0.32(1)	0.072(4)	1.30	−1.34	0.110(9)	2.54(5)
`Spo3`	3.00	25.220 / 9	2.24(3)	−0.33(1)	0.075(4)	1.31	−1.35	0.111(9)	2.52(5)
`Spp3`	3.00	21.550 / 9	2.23(3)	−0.34(1)	0.078(5)	1.31	−1.35	0.112(8)	2.51(5)
`Sfm3`	3.00	27.120 / 8	2.33(9)	−0.24(9)	0.203(159)	1.27	−0.68(75)	0.090(61)	2.59(13)
`Sfo3`	3.00	24.190 / 8	2.31(10)	−0.26(10)	0.180(175)	1.28	−0.82(82)	0.095(64)	2.57(14)
`Sfp3`	3.00	21.180 / 8	2.28(12)	−0.28(11)	0.159(188)	1.29	−0.95(87)	0.099(65)	2.55(15)

Table 5
Parameters from our fits to the nucleon mass alone. All keys start with `N..` indicating that no σ-term data has been included. The remaining character sequence has the same meaning as in Table 4.

Key	$(r_0 m_\pi)^2_{\max}$	χ^2_r	$r_0 M_0$	c_1/r_0	e^r_1/r_0^3	c_2/r_0	c_3/r_0	$r_0\sigma_{\text{phys}}$	r_0 [1/GeV]
`Nmo1`	1.30	4.760 / 4	2.19(9)	−0.39(6)	−0.155(11)	1.33	−2.42	0.111(40)	2.48(10)
`Noo1`	1.30	3.510 / 4	2.23(9)	−0.34(6)	−0.030(11)	1.32	−1.88	0.103(35)	2.50(9)
`Npo1`	1.30	4.450 / 4	2.26(9)	−0.29(6)	0.088(11)	1.31	−1.35	0.096(40)	2.53(10)
ave.	1.30	$\chi^2_r < 1.3$	2.23(9)	−0.34(6)	−0.032(11)	–	–	0.10(4)	2.50(10)
`Nfo1`	1.30	3.510 / 3	2.23(10)	−0.34(8)	−0.024(133)	1.32	−1.85(58)	0.103(50)	2.51(12)
`Nmo2`	1.60	5.280 / 6	2.20(7)	−0.38(4)	−0.153(8)	1.32	−2.41	0.109(23)	2.49(7)
`Noo2`	1.60	4.200 / 6	2.23(7)	−0.34(4)	−0.031(8)	1.32	−1.87	0.103(21)	2.51(6)
`Npo2`	1.60	5.170 / 6	2.26(7)	−0.30(4)	0.086(7)	1.31	−1.35	0.097(24)	2.52(7)
ave.	1.60	$\chi^2_r < 1.3$	2.23(7)	−0.34(4)	−0.022(8)	–	–	0.103(22)	2.51(6)
`Nfo2`	1.60	4.200 / 5	2.23(8)	−0.34(6)	−0.029(132)	1.32	−1.87(58)	0.103(26)	2.51(7)
`Nmo3`	3.00	35.320 / 8	1.92(4)	−0.57(1)	−0.191(9)	1.47	−2.68	0.156(11)	2.24(8)
`Noo3`	3.00	17.010 / 8	2.04(4)	−0.46(1)	−0.030(8)	1.41	−2.00	0.138(9)	2.35(6)
`Npo3`	3.00	11.140 / 8	2.14(4)	−0.37(1)	0.099(7)	1.36	−1.40	0.121(8)	2.43(4)
`Nfo3`	3.00	10.810 / 7	2.18(11)	−0.34(10)	0.150(156)	1.34	−1.15(69)	0.114(43)	2.46(12)

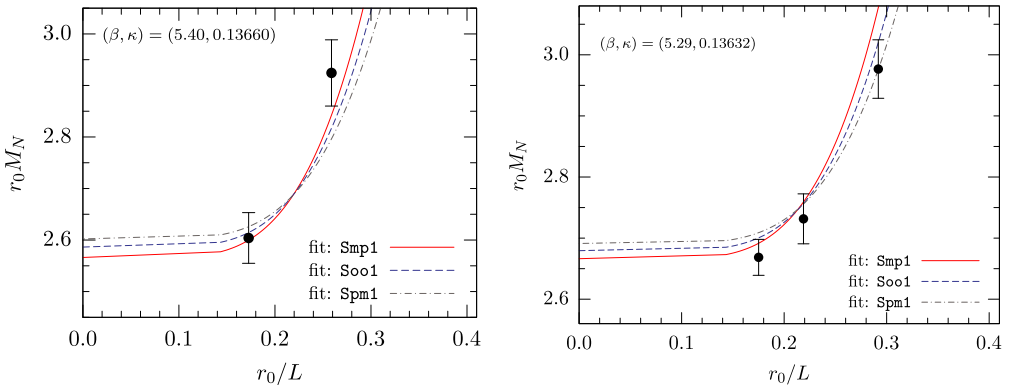

Fig. 10. Volume dependence of our nucleon mass data at $(\beta,\kappa) = (5.29, 0.13632)$ (left) and $(5.40, 0.13660)$ (right) resulting from different combined fits, labeled `Smp1`, `Soo1` and `Spm1` in Table 4. They illustrate the maximum variation of the finite-volume corrections for all our combined fits [for $(r_0 m_\pi)^2 < 1.3$] with the parameters c_3 and $\bar{l}_3$.

of the fit parameters on this external bias. Table 4 summarizes the results for the combined fits and Table 5 those for the stand-alone fits.

The two tables have to be read as follows: Each line is the result for one particular fit. In the first column, a unique key is assigned to each fit. Keys starting with `N` ("no σ") refer to stand-alone fits to the nucleon mass data [i.e., Eq. (10)], while keys starting with `S` ("with σ") signify combined fits [Eq. (11)]. The second and third characters are either `m`, `o`, `p` or `f`, depending on the values assigned to the parameters c_3 and $\bar{l}_3$ (see Section 3.3). If the second (third) character is an `o`, c_3 ($\bar{l}_3$) was fixed to $c_3 = -4.7$ GeV^{-1} ($\bar{l}_3 = 3.2$); if instead this character is `p` (`m`), c_3 and $\bar{l}_3$ were fixed to these values, plus (minus) one standard deviation. If the second character is `f`,

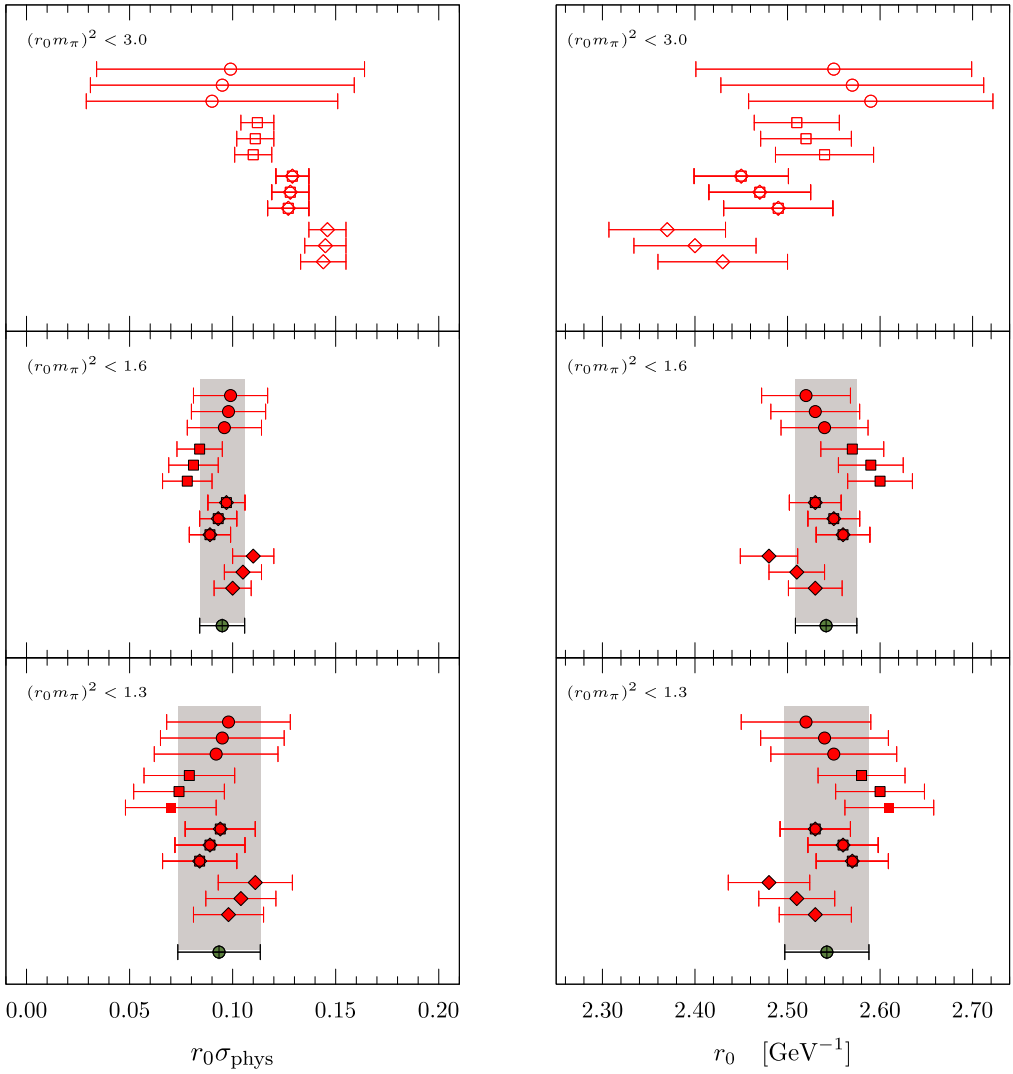

Fig. 11. Values for $r_0\sigma$ at the physical point (left) and r_0 (right) from the combined fits listed in Table 4. From top to bottom, panels are ordered according to a decreasing upper limit for $(r_0 m_\pi)^2$. Within each panel, data points are grouped with respect to the values chosen for c_3 and $\bar{l}_3$: Different (red) symbols refer to different values for c_3 (circles: $c_3 =$ free; squares: $c_3 = -4.7 + 1.3$; polygons: $c_3 = -4.7$; diamonds: $c_3 = -4.7 - 1.3$, all in GeV^{-1}), while triples of neighboring points (same symbol) refer to different values of $\bar{l}_3 = 3.2 + 0.8$, 3.2, $3.2 - 0.8$ (from top to bottom). Open symbols refer to poor fits ($\chi^2_r > 2.0$), full symbols to good fits ($\chi^2_r < 2.0$) and black-framed full symbols to fits where $\chi^2_r < 1.3$. If applicable, gray error bands are shown for weighted averages (green symbol at the bottom of each band) of the black-framed points. (For interpretation of the references to color in this figure legend, the reader is referred to the web version of this article.)

c_3 was not fixed but left as a free fit parameter. Since c_2 is known to a much better precision than c_3 [see Eq. (13)] it is not varied, but always set to its phenomenological value $c_2 = 3.3$ GeV^{-1}. Each key ends with an integer labeling, in increasing order, the upper limit $(r_0 m_\pi)^2_{\rm max}$ of the fit interval

$$(r_0 m_\pi)^2 < (r_0 m_\pi)^2_{\max}, \tag{B.1}$$

where $(r_0 m_\pi)^2_{\max}$ is either 1.3, 1.6 or 3.0 (given in the second column). In all cases we require $L/r_0 > 3$. To reduce the finite-volume effect in the pion mass, we exclude data points for all those (β, κ) combinations for which there is not at least one value for $r_0 m_\pi$ available that satisfies $m_\pi L > 3.5$.

All (fixed and floating) fit parameters listed in Tables 4 and 5 are given in units of r_0. The corresponding self-consistent physical value of r_0—reached iteratively for each fit (see Eq. (9))—is given in the last column in GeV^{-1}. That is, if one is interested in the physical value for a particular fit parameter, this parameter has to be multiplied by the corresponding power of r_0 given at the end of the same line. In Table 4 we also give weighted averages of the fit parameters for fits with a $\chi^2_r < 1.3$ (see lines starting with "ave.").

Let us now comment our fits. The fact that our fits with $(r_0 m_\pi)^2 < 1.6$ yield (in the majority of cases) χ^2_r-values around one indicates that the constraint $L/r_0 > 3.0$ on the spatial lattice extension has been sufficient to correct for the finite-volume effect in the data. This can be seen also from Fig. 10, where we compare data for $r_0 M_N$ at fixed (β, κ) but different L/r_0 to the fitted function at the corresponding $r_0 m_\pi$. If we had relaxed the constraint $L/r_0 > 3$, the finite-volume effect could not be completely compensated for data points with $L/r_0 \leqslant 3$. This is, for example, the case for our points at $(\beta, \kappa) = (5.40, 0.13640)$ from a $24^3 \times 48$ lattice.

Looking at the fit parameter e^r_1, our fits are less robust, however. In fact, the sign of e^r_1 is strongly correlated with the value we choose for c_3. If we set, for example, $c_3 = -4.7 + 1.3\ \mathrm{GeV}^{-1}$ all fits result in a positive e^r_1, while, if we set $c_3 = -4.7\ \mathrm{GeV}^{-1}$ or $c_3 = -4.7 - 1.3\ \mathrm{GeV}^{-1}$, e^r_1 comes always out negative. The value we choose for $\bar{l}_3$ does not affect the sign of e^r_1, yet $\bar{l}_3$ has a minor effect on e^r_1's absolute value. To our knowledge, nothing is really known about the sign of e^r_1, so we do not restrict it. From our data we can say it tends to be negative if $c_3 \leqslant -4.7\ \mathrm{GeV}^{-1}$ and positive if $c_3 \geqslant -3.4\ \mathrm{GeV}^{-1}$. If we leave c_3 as free fit parameter, we obtain values around $-5.0\ \mathrm{GeV}^{-1}$ for c_3 ($\pm 1.5\ \mathrm{GeV}^{-1}$ statistical uncertainty), and e^1_r is consistent with zero within errors. This is found for fits where $(r_0 m_\pi)^2_{\max}$ is either 1.6 or 1.3. Interestingly, the range of fitted values for e^r_1 lies in the ballpark expected from BChPT (see Eq. (A.25)).

A correlation with c_3 is also seen for $r_0 \sigma_{\mathrm{phys}}$ and r_0 (see columns 9 and 10 in Tables 4 and 5). For larger, i.e., less negative values of c_3, the results for $r_0 \sigma_{\mathrm{phys}}$ tend to smaller numbers, while r_0 tends to larger values.

For the reader's convenience, we visualize the variation of the values for r_0 and $r_0 \sigma_{\mathrm{phys}}$ in Fig. 11 (only for results from Table 4). From top to bottom, panels are ordered with decreasing $(r_0 m_\pi)^2_{\max}$, while within each panel, points are grouped according to the values chosen for c_3 and $\bar{l}_3$. Symbols distinguish different c_3, neighboring points with the same symbol are for different $\bar{l}_3$. The color intensity of each point is related to the χ^2_r-value of each point. When applicable each panel also shows the corresponding weighted average.

References

[1] R. Koch, Z. Phys. C 15 (1982) 161.
[2] M. Pavan, et al., PiN Newslett. 16 (2002) 110, hep-ph/0111066.
[3] J. Gasser, H. Leutwyler, M. Sainio, Phys. Lett. B 253 (1991) 252.
[4] B. Borasoy, U.-G. Meissner, Annals Phys. 254 (1997) 192, hep-ph/9607432.
[5] J.M. Alarcon, J. Martin Camalich, J.A. Oller, arXiv:1110.3797, 2011.
[6] R. Babich, et al., Phys. Rev. D 85 (054510) (2012), arXiv:1012.0562.

[7] G.S. Bali, et al., QCDSF Collaboration, Phys. Rev. D 85 (054502) (2012), arXiv:1111.1600.
[8] S. Dinter, et al., arXiv:1202.1480, 2012.
[9] R. Horsley, et al., Phys. Rev. D 85 (034506) (2012), arXiv:1110.4971.
[10] S. Dürr, et al., Phys. Rev. D 85 (014509) (2012), arXiv:1109.4265.
[11] P. Shanahan, A. Thomas, R. Young, arXiv:1205.5365, 2012.
[12] G. Bali, J. Najjar, 2012, in preparation.
[13] G. Colangelo, S. Dürr, C. Haefeli, Nucl. Phys. B 721 (2005) 136, hep-lat/0503014.
[14] J.A. McGovern, M.C. Birse, Phys. Rev. D 74 (2006) 097501, hep-lat/0608002.
[15] G. Colangelo, et al., Eur. Phys. J. C 71 (1695) (2011), arXiv:1011.4408.
[16] U.-G. Meissner, PoS LAT2005 (2006) 009, hep-lat/0509029.
[17] U.-G. Meissner, private communication.
[18] N. Fettes, PhD thesis, Universität, Bonn, Germany, 2000.
[19] V. Bernard, U.-G. Meissner, Phys. Lett. B 639 (2006) 278, hep-lat/0605010.
[20] D.B. Leinweber, et al., Phys. Rev. D 61 (2000) 074502, hep-lat/9906027.
[21] S.R. Beane, Nucl. Phys. B 695 (2004) 192, hep-lat/0403030.
[22] D.B. Leinweber, A.W. Thomas, R.D. Young, Nucl. Phys. A 755 (2005) 59, hep-lat/0501028.
[23] M.R. Schindler, PhD thesis, Johannes Gutenberg-Universität, Mainz, Germany, 2007.
[24] S. Güsken, et al., TXL Collaboration, Phys. Rev. D 59 (1999) 054504, hep-lat/9809066.
[25] M. Procura, T.R. Hemmert, W. Weise, Phys. Rev. D 69 (2004) 034505, hep-lat/0309020.
[26] M. Procura, et al., Phys. Rev. D 73 (2006) 114510, hep-lat/0603001.
[27] H. Ohki, et al., Phys. Rev. D 78 (054502) (2008), arXiv:0806.4744.
[28] R. Young, A. Thomas, Phys. Rev. D 81 (014503) (2010), arXiv:0901.3310.
[29] K.-I. Ishikawa, et al., PACS-CS Collaboration, Phys. Rev. D 80 (054502) (2009), arXiv:0905.0962.
[30] C. Alexandrou, et al., ETM Collaboration, Phys. Rev. D 80 (114503) (2009), arXiv:0910.2419.
[31] D.B. Leinweber, A.W. Thomas, R.D. Young, Phys. Rev. Lett. 92 (2004) 242002, hep-lat/0302020.
[32] C. Aubin, et al., Phys. Rev. D 70 (2004) 094505, hep-lat/0402030.
[33] M. Göckeler, et al., PoS LAT2005 (2006) 063, hep-lat/0509196.
[34] M. Göckeler, et al., Phys. Rev. D 73 (2006) 014513, hep-ph/0502212.
[35] P. Fritzsch, et al., arXiv:1205.5380, 2012.
[36] R.G. Edwards, B. Joo, SciDAC Collaboration, LHPC Collaboration, UKQCD Collaboration, Nucl. Phys. B (Proc. Suppl.) 140 (2005) 832, hep-lat/0409003.
[37] P.A. Boyle, Comp. Phys. Comm. 180 (2009) 2739.
[38] Y. Nakamura, H. Stüben, PoS LATTICE2010 (2010) 040, arXiv:1011.0199.
[39] J. Gasser, H. Leutwyler, Annals Phys. 158 (1984) 142.
[40] S. Bellucci, J. Gasser, M. Sainio, Nucl. Phys. B 423 (1994) 80, hep-ph/9401206.
[41] M. Dorati, T.A. Gail, T.R. Hemmert, Nucl. Phys. A 798 (96) (2008), nucl-th/0703073.
[42] T. Becher, H. Leutwyler, JHEP 0106 (2001) 017, hep-ph/0103263.
[43] A. Ali Khan, et al., QCDSF-UKQCD Collaboration, Nucl. Phys. B 689 (2004) 175, hep-lat/0312030.
[44] M. Schindler, et al., Phys. Lett. B 649 (2007) 390, hep-ph/0612164.
[45] T. Becher, H. Leutwyler, Eur. Phys. J. C 9 (1999) 643, hep-ph/9901384.